FULL PAPER

WILEY Applied Organometallic Chemistry

Polymer complexes. LXIX. Some divalent metal(II) polymer complexes of potentially bidentate monomer N-[4-(5-methyl-isoxazol-3-ylsulfamoyl)-phenyl]-acrylamide: Synthesis, spectroscopic characterization, thermal properties, antimicrobial agents and DNA studies

A.Z. El-Sonbati[1] (iD) | M.A. Diab[1] (iD) | Sh.M. Morgan[2] (iD) | A.M. Eldesoky[3,4] | M.Z. Balboula[1]

[1] Chemistry Department, Faculty of Science, Damietta University, Egypt

[2] Environmental Monitoring Laboratory, Ministry of Health, Port Said, Egypt

[3] Engineering Chemistry Department, High Institute of Engineering & Technology (New Damietta), Egypt

[4] Al-Qunfudah Center for Scientific Research (QCSR), Chemistry Department, Al-Qunfudah University College, Umm Al-Qura University, Kingdom of Saudi Arabia

Correspondence

A. Z. El-Sonbati, Chemistry Department, Faculty of Science, Damietta University, Egypt

Email: elsonbatisch@yahoo.com

Monomer of N-[4-(5-methyl-isoxazol-3-ylsulfamoyl)-phenyl]-acrylamide (HL) and some transition metal polymeric complexes of the general formula $\{[M(HL)(OH_2)_2(OCOCH_3)_2] xH_2O\}_n$ (M = Co(II), x = 2; Ni(II), x = 3; Mn(II), x = 2) and $[Cd(HL)_2(OCOCH_3)_2]$ were synthesized and characterized by elemental analysis, IR, UV spectroscopy, conductance measurements, magnetic susceptibility, thermogravimetric analyses and X-ray diffraction analysis. In all polymer complexes, the spectral data revealed that the ligand act as bidentate neutral molecule and coordinate to metal ion through enolic sulphonamide OH and isoxazol-N. In all polymer complexes, the spectral data revealed that the ligand act as bidentate neutral molecule and coordinate to metal ion through enolic sulphonamide OH and isoxazol-N. The molar conductance data revealed that the polymer complexes are non-electrolytes while UV-vis and magnetic measurements data have been shown that the polymer complexes have octahedral geometry. All the studies revealed coordination six for the metals in all the polymer complexes and octahedral structures were suggested. The inhibitive effect of HL against C38 steel was investigated in 2 M HCl solution (tafel polarization, electrochemical impedance spectroscopy (EIS) and electrochemical frequency modulation (EFM) methods). The type of HL is mixed inhibitor whose adsorption habit onto C38 steel.

KEYWORDS

corrosion inhibition, molecular docking, polymer complexes, thermal properties, thermodynamic parameters

1 | INTRODUCTION

Sulphadrugs have a broad spectrum effect against many bacterial strains[1] and they are widely used in treatment of various bacterial infections.[2–4] Metal of drug interactions were emerged as a new field of study.[5–8]

Also, the metal chelates of sulphadrugs compounds showed strong bacteriostatic efficiency than the sulphadrugs compounds.[9,10]

Coordination supramolecules and polymers based on transition metals compounds were discussed.[11,12] The styling of coordination polymers is based on transition

metals. The polymer complexes of sulphadrugs with a series of metal ion were studied.[13–19] DNA is the main target molecule for most anticancer and antiviral therapies according to cell biology.[20] The interactions of DNA with transition metal complexes and different types of interaction of these metal complexes with DNA have been informed.

Organic inhibitors are applied extensively to keep metals from corrosion in many aggressive acidic media; these organic inhibitors are compounds containing nitrogen, sulfur or oxygen.[21,22] Regrettably, most of the organic used inhibitors are very expensive and health hazards. The toxicity of these organic inhibitors restricts the field of their application. So it was necessary to find low-cost inhibitors of the non-hazardous type for the protection of metals against corrosion. These requirements were satisfied by sulfa drugs compounds which have a large number of functional adsorption centers (e.g. $-NH_2$ group, $-SO_2-NH-$ group, O and/or N- hetero atoms and aromatic rings).

In this study describes the coordination behavior of monomer with Co(II), Ni(II), Mn(II) and Cd(II) acetate. The structure of the studied polymer complexes is elucidated using elemental analysis, IR, UV spectroscopy, conductance measurements, magnetic susceptibility, X-ray diffraction and thermal analysis measurements. Thermal decomposition and thermodynamic parameters of the polymer complexes are discussed. The protection effect and electrochemical habit of HL for C38 steel contain 2 M HCl acid is given by the tafel polarization, EIS and EFM tests are studied.

2 | EXPERIMENTAL

The experimental technique has been described previously.[11,12,18]

2.1 | Material and methods

4-Amino-N-(5-methyl-isoxazol-3-yl)-benzenesulfonamide was bought Aldrich and used without further purification. Acryloyl chloride (Aldrich Chemical Co. Inc.) was used without further purification. 2,2′-Azobisisobutyronitrile (AIBN) was purified by dissolving in hot ethanol and filtering.[11] The solution was left to cool. Co(OCOCH$_3$)$_2$. 4H$_2$O, Ni(OCOCH$_3$)$_2$. 4H$_2$O, Mn(OCOCH$_3$)$_2$. 4H$_2$O and Cd(OCOCH$_3$)$_2$.2H$_2$O (Sigma Aldrich), and sodium carbonate (Merck) (BDH). Organic solvents were spectroscopic pure from BDH included ethanol, diethyl ether and dimethylformamide.

2.2 | Preparation of monomer

HL monomer was prepared by the reaction of equimolar amounts of acryloyl chloride and 4-amino-N-(5-methyl-isoxazol-3-yl)-benzenesulfonamide in dry benzene until the evolution of hydrogen chloride ceased,[18] forming a white powder of monomer yield ~ 65 % and m.p. 220 °C. Microanalysis for $C_{13}H_{14}N_3SO_4$; Found: C, 50.72; H, 4.65; N, 13.85; S, 10.63. Calc. for HL: C, 50.81; H, 4.23; N, 13.68; S, 10.42%. Mass spectrum, the ion of m/z = 307 undergoes fragmentation to a stable peak at m/z = 252, 173, 97 and 82 by losing C_2H_3CO, C_5H_5N, CSO_2 and NH atoms, respectively. IR [υ_{max}. (cm^{-1}) (KBr)]: 3283-3178 (N-H str. sym.), 3055 (=C-H str.), 2977 (C-H str. -CH$_3$), 2874 (C-H str.- CH$_2$), 1518, 1591 (C=C Ph. ring), 2776 (C-H str. sym.) 1473 (oxazole ring str.), 1369 (S=O asym.), 1162 (S=O sym.), 1095 (C-H) oxazole), 1033 (ring skeletol oxazol), 795 cm^{-1} (N-H wag.), 1390, 1165 cm^{-1} (N-O isoxazole).

^{1}H NMR: δ (ppm) 7.43-7.80 (d, Ar, 4H), 6.10, 6.30 (s, CH$_2$=, 2H), 5.80 (s, =CH, 1H), 10.65, 10.85 (s, SO$_2$NH, 1H, exchangeable with D$_2$O), 5.18 (s, CONH, 1H, exchangeable with D$_2$O), 6.26 (s, =CH oxazole ring, 1H) and 2.10 (s, CH$_3$, 3H). ^{13}C NMR (DMSO-d$_6$): δ (ppm) 170.0 (^{3}C), 168.0 (^{10}C), 158.6 (^{7}C), 153.8 (^{4}C), 132.6 (^{1}C), 127.6 (^{2}C), 128.8 (^{5,9}C), 126.2 (^{12}C), 119 (^{6,8}C) and 13.7 (^{13}C) (Figure 1)

2.3 | Polymerization

Monomer was homopolymerized by the method described by Diab, El-Sonbati and co-workers.[11,12,18] The IR spectrum of the homopolymer was almost the same as that of the monomer except the absence of a peak at 1585 cm^{-1} which assigned to the participation of (C=C) in the polymerization.

2.4 | Isolation of polymer complexes

Polymer complexes were prepared by refluxing the monomer with Co(II), Ni(II), Mn(II) and Cd(II) acetate in DMF as a solvent, and 0.1 % (w/v) initiator (2,2′-azobisisobutyronitrile (AIBN)). The resulting mixture was heated at reflux for ~ 8 hrs. The hot solution was precipitated by pouring in large excesses of distilled water containing dilute hydrochloric acid, to remove the metal salts that were incorporated into the polymer complexes. The polymer complexes (Figure 1) were filtered, washed with water, and dried in a vacuum oven at 40 °C for several days.

2.4.1 | {[Co(HL)(OCOCH$_3$)$_2$(H$_2$O)$_2$] 2H$_2$O}$_n$ (1)

Anal. calcd. for **C$_{17}$H$_{27}$N$_3$SO$_{12}$Co**: C, 36.70; H, 4.14; N, 7.55; S, 5.76; Co, 10.60%. Experimental: C, 36.64; H, 4.04; N, 7.35; S, 5.56; Co, 10.91%. IR [υ_{max}. (cm^{-1}) (KBr)]: 3060 (OH str. enolic.), 2930 (C-H str. -CH$_3$), 2927 (C-H str.- CH$_2$), 1475,
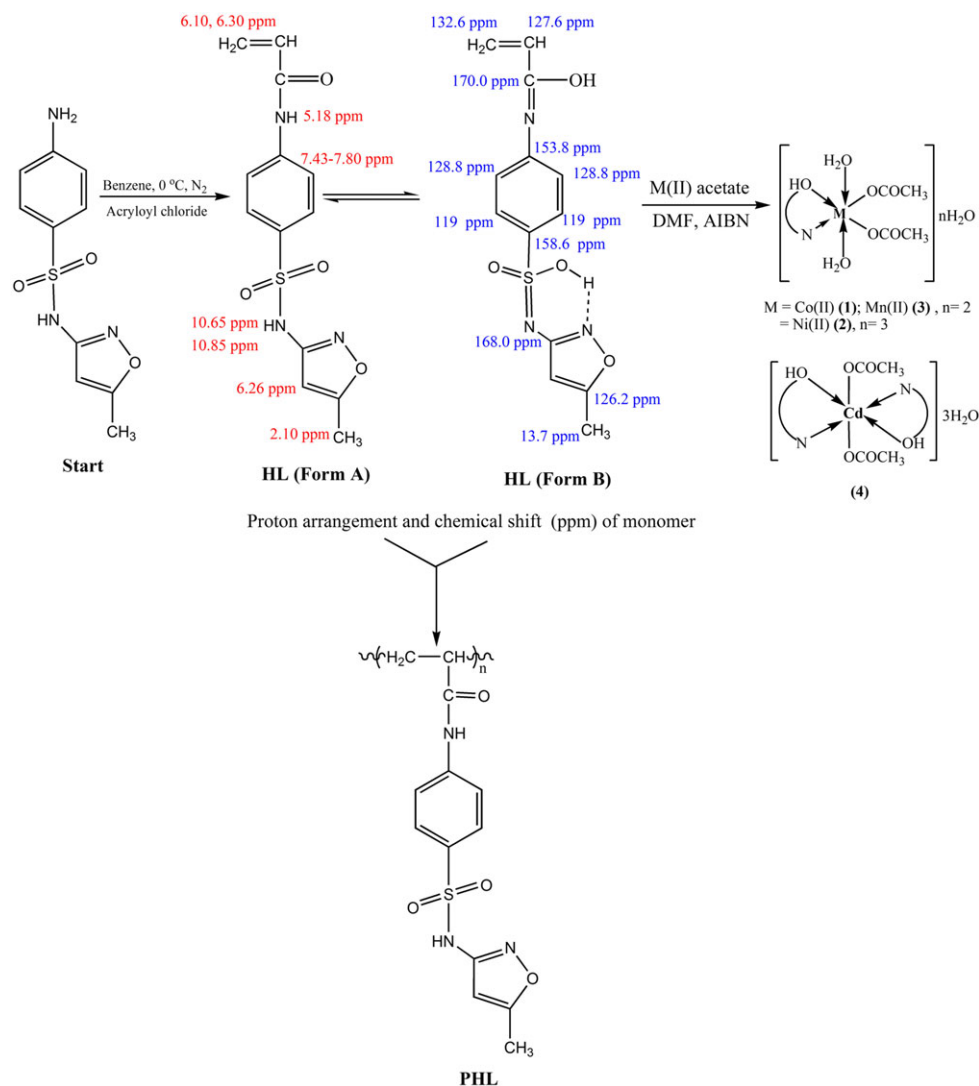
FIGURE 1 Structure of the monomer, homopolymer (PHL) and polymer complexes

1412 (oxazole ring str.), 1311 (S=O asym.), 1162 (S=O sym.), 1094 (C-H) oxazole), 1020 (ring skeletol oxazol), 1531 (CH$_3$COO$^-$ sym.), 1311 (CH$_3$COO$^-$ asym.), 3315 (OH water), 835 (OH rocking water), 794 (N-H wag.). 592 (Co-O), 440 (Co-N). Molar Cond. (10^{-3} M, DMSO): 20.33 Ω^{-1} cm^2 mol^{-1}. $\mu_{eff.}$ = 4.80 BM., UV-Vis. (cm^{-1}): Racah parameter < free ion value, β < 1, υ_2/υ_1 = 2.04.

2.4.2 | {[Ni(HL)(OCOCH$_3$)$_2$(H$_2$O)$_2$] 3H$_2$O}$_n$ (2)

Anal. calcd. for **C$_{17}$H$_{29}$N$_3$SO$_{13}$Ni**: C, 35.56; H, 4.01; N, 7.32; S, 5.58; Ni, 10.23%. Experimental: C, 35.44; H, 3.84; N, 7.04; S, 5.35; Ni, 10.60%. IR [$\upsilon_{max.}$ (cm^{-1}) (KBr)]: 3080 (OH str. enolic.), 2908 (C-H str. -CH$_3$), 2880 (C-H str.-CH$_2$), 1481, 1411 (oxazole ring str.), 1307 (S=O asym.), 1132 (S=O sym.), 1095 (C-H) oxazole), 1025 (ring skeletol oxazol), 1536 (CH$_3$COO$^-$ sym.), 1308 (CH$_3$COO$^-$ asym.), 3404 (OH water), 835 (OH rocking water), 764 (N-H wag.). 594 (Ni-O), 445 (Ni -N). Molar Cond. (10^{-3} M, DMSO): 10.50 Ω^{-1} cm^2 mol^{-1}. $\mu_{eff.}$ = 2.88 BM,. UV.vis. (cm^{-1}): Racah parameter < free ion value, β < 1, υ_2/υ_1 = 1.59.

2.4.3 | {[Mn(HL)(OCOCH$_3$)$_2$(H$_2$O)$_2$] 2H$_2$O}$_n$ (3)

Anal. calcd. for **C$_{17}$H$_{27}$N$_3$SO$_{12}$Mn**: C, 36.96; H, 4.17; N, 7.61; S, 5.80; Mn, 9.95%. Experimental: C, 36.88; H, 4.11; N, 7.44; S, 5.65; Mn, 10.18%. IR [$\upsilon_{max.}$ (cm^{-1}) (KBr)]: 3108 (OH str. enolic.), 2910 (C-H str. -CH$_3$), 2890(C-H str.- CH$_2$), 1470, 1396 (oxazole ring str.), 1330 (S=O asym.), 1162 (S=O sym.), 1088 (C-H) oxazole), 1034 (ring skeletol oxazol), 1524 (CH$_3$COO$^-$ sym.), 1330 (CH$_3$COO$^-$ asym.), 3265 (OH water), 835 (OH rocking water), 796 (N-H wag.). 569 (Mn-O), 480 (Mn-N). Molar Cond. (10^{-3} M, DMSO): 8.44 Ω^{-1} cm^2 mol^{-1}. $\mu_{eff.}$ = 5.91 B.M., UV.vis. (cm^{-1}):

Racah parameter < free ion value, $\beta < 1$, $F_2 = 1166$, $F_4 = 97$, $B = 68$, $C = 3401$.

2.4.4 | $\{[Cd(HL)_2(OCOCH_3)_2] \cdot 3H_2O\}_n$ (4)

Anal. calcd. for $C_{30}H_{38}N_6S_2O_{15}Cd$: C, 40.07; H, 3.56; N, 9.35; S, 7.12; Cd, 12.51%. Experimental: C, 39.97; H, 3.44; N, 9.15; S, 6.88; Cd, 13.04%. IR [$\upsilon_{max.}$ (cm^{-1}) (KBr)]: 3112 (OH str. enolic.), 2925 (C-H str. -CH$_3$), 2890 (C-H str.- CH$_2$), 1473, 1404 (oxazole ring str.), 1313 (S=O asym.), 1164 (S=O sym.), 1067 (C-H) oxazole), 1055 (ring skeletol oxazol), 1535 (CH$_3$COO$^-$ sym.), 1313 (CH$_3$COO$^-$ asym.), 3270 (OH water), 792 (N-H wag.). 586 (Cd-O), 435 (Cd-N). Molar Cond. (10^{-3} M, DMSO): 15.30 Ω^{-1} cm^2 mol^{-1}. $\mu_{eff.}$ = diamagnetic

2.5 | Biological activity investigation

For this investigation the agar well diffusion method was applied.[23,24] The antibacterial activities of the investigated compounds were tested against three local Gram positive bacterial species (*Bacillus cereus*, *Staphylococcus aureus* and *Enterococcus faecalis*) and three local Gram negative bacterial species (*Escherichia coli*, *Klebsiella pneumoniae* and *Pseudomonas aeruginosa*) on nutrient agar medium. Also, the antifungal activities were tested against three local fungal species (*Aspergillus niger*, *Fusarium oxysporum* and the yeast *Candida albicans*) on DOX agar medium. The concentrations of each solution were 50, 100 and 150 μg/ml in buffered dimethylformamide (DMF) solution. By using a sterile cork borer (10 mm diameter), wells were made in agar medium plates previously seeded with the test microorganisms. 200 μl of each compound was applied in each well. The agar plates were kept at 4 °C for at least 30 min to allow the diffusion of the compound to agar medium. The plates were then incubated at 37 °C or 30 °C for bacteria and fungi, respectively. The diameters of inhibition zone were determined after 24 h and 7 days for bacteria and fungi, respectively, taking the consideration of the control values (DMF). Dimethylformamide (DMF) was used as a blank and penicillin was used as the antibacterial standard drug and miconazole was used as the antifungal standard drug.

2.6 | DNA binding measurements

The binding properties of the monomer (HL) and complexes (1–4) to CT-DNA have been studied using electronic absorption spectroscopy. The stock solution of CT-DNA was prepared in 5 mM Tris–HCl/50 mM NaCl buffer (pH = 7.2), which a ratio of UV absorbance at 260 and 280 nm (A$_{260}$/A$_{280}$) of ca. 1.8–1.9, indicating that the DNA was sufficiently free of protein and the concentration was determined by UV absorbance at 260 nm ($\mathcal{E} = 6600$ M^{-1} cm^{-1}).[24] Electronic absorption spectra were carried out using 1 cm quartz cuvettes at 25 °C by fixing the concentration of Schiff base or complexes (1.00×10^{-3} mol L^{-1}), while gradually increasing the concentration of CT-DNA (0.00 to 1.30×10^{-4} mol L^{-1}). An equal amount of CT-DNA was added to both the compound solutions and the references buffer solution to eliminate the absorbance of CT-DNA itself. The intrinsic binding constant (K$_b$) of the compound with CT-DNA was determined using the following equation:[24]

$$\frac{[DNA]}{(\varepsilon_a - \varepsilon_f)} = \frac{[DNA]}{(\varepsilon_b - \varepsilon_f)} + \frac{1}{K_b(\varepsilon_a - \varepsilon_f)} \tag{1}$$

where [DNA] is the concentration of CT-DNA in base pairs, ϵ_a is the molar extinction coefficient observed for the A$_{obs}$/[compound] at the given DNA concentration, ϵ_f is the molar extinction coefficient of the free compound in solution and ϵ_b is the molar extinction coefficient of the compound when fully bond to DNA. In plots of [DNA]/(ϵ_a–ϵ_f) versus [DNA], K$_b$ is given by the ratio of the slope to the intercept.

2.7 | Measurements

Microanalyses of carbon, hydrogen, nitrogen and sulfur were carried out using a CHNS-932 (LECO) Vario Elemental Analyzer at the Microanalytical Center. ^{1}H NMR spectra were on record with a 330 MHz Varian-Oxford Mercury. Infrared spectra were recorded as KBr discs using a Perkin-Elmer 1340 spectrophotometer. Mass spectra were recorded by the EI technique at 70 eV using MS-5988 GS-MS Hewlett-Packard. Ultraviolet-visible (UV-Vis) spectra of the compounds were recorded in nujol mulls using a Unicom SP 8800 spectrophotometer. Magnetic moment of the prepared solid complexes was determined at room temperature using the Gouy's method. Mercury(II) (tetrathiocyanato)cobalt(II), [Hg{Co(SCN)$_4$}], was used for the calibration of the Gouy tubes. Diamagnetic corrections were calculated from the values given by Selwood[25] and Pascal's constants.

Magnetic moments were calculated using the equation, $\mu_{eff.} = 2.84 \, [Tc_M^{coor.}]^{1/2}$. The conductance was achieved using Sergeant Welch scientific Co., Skokie, IL, USA. Simultaneous Thermal Analyzer (STA) 6000 system was used in computing the thermal studies by thermogravimetric analysis (TGA) method. Thermal properties were studied from 50 °C to 800 °C at the heating rate of 15 °C/min under dynamic nitrogen atmosphere. X-ray diffraction analysis of compounds powder forms was recorded on X-ray diffractometer analysis in the range of diffraction angle 2θo = 4–80o.[24] This analysis was carried out using

CuKα radiation (λ = 1.540598 Å). The applied voltage and the tube current are 40 kV and 30 mA, respectively.

Docking calculations were carried out on receptors of crystal structures of *Escherichia coli* (3t88) and *Staphylococcus aureus* (3q8u) proteins models. The MMFF94 Force field was used for energy minimization of compound molecule using Docking Server. Affinity (grid) maps of 20 × 20 × 20 Å grid points and 0.375 Å spacing were generated using the Autogrid program.[26–28] Auto Dock parameter set- and distance-dependent dielectric functions were used in the calculation of the van der Waals and the electrostatic terms, respectively.

2.8 | Electrochemical tests

Electrochemical tests were lead to three electrodes cell thermostatic utilized a Gamrypotentiostat/galvanostat/ZRA (model PCI300/4). A saturated calomel and platinum electrode were utilized as reference and auxiliary electrodes. The C38 steel electrodes were 10 x 10 ml and were welded with a copper wire on one side. All method was done at temperature (30 ± 1 °C). The potentiodynamic diagrams were measured from -50 to 50 V at a rate scan 1 mV S^{-1} after the steady state is approached (30 min) and the open potential circuit was observed after putted the electrode for 15 min in the solution test.

EFM and EIS tests were obtained by utilized the same methods as before with a Gamry framework system depends on ESA400. EchemAnalyst 5.5 Software was utilized for drawing, graphing and fitting data. EIS tests were done in a range of frequency of 100 kHz to 10 mHz with amplitude of 5 mV peak-to-peak ac signals utilized at respective for potential corrosion. EFM had done utilized 2 frequencies 2 and 5 Hz. The frequency base was 1 Hz. In this research, we utilized a signal perturbation with amplitude of 10 mV for both frequencies perturbation of 2 and 5 Hz.

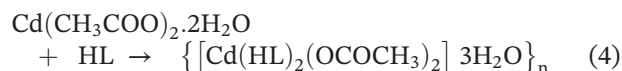# 3 | RESULTS AND DISCUSSION

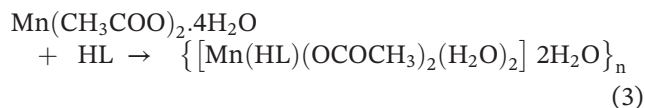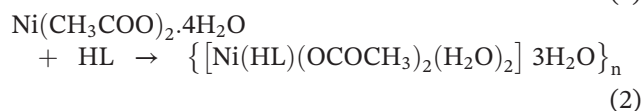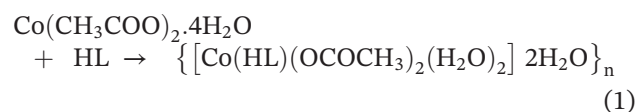## 3.1 | Characterization of monomer

The monomer is characterized as in Section 2. The monomer was then polymerized as in Section 2. The monomer was then polymerized by radical polymerization initiated by 2,2′-azobisisobutyronitrile (AIBN). The homopolymer has been characterized by various techniques.[16,18] The proposed formula was confirmed by mass spectrum of monomer showing a peak at 307 amu corresponding to the molecular ion peak of the monomer moiety ($[C_{13}H_{13}N_3O_4S]$ atomic mass 307 amu). The observed peak was in good agreement with the proposed formula as indicated by the analytical data. The results showed a possible arrangement between the start and monomer (forms A and B) with receptors of crystal structures of

Escherichia coli (3t88) and *Staphylococcus aureus* (3q8u). The docking study showed a favorable interaction between start and forms A and B with the receptors (3t88 and 3q8u) as shown in Figures 2–4 and energy is given in Table 1. 2D plot curves for start and forms A and B of monomer are shown in Figures 5–7.

3.2 | Structure and characterization of polymer complexes

3.2.1 | Elemental analyses

The analytical data of the isolated polymer complexes are shown in Section 2. The formation of these polymer complexes may propose according to the following equations:

$$Co(CH_3COO)_2.4H_2O + HL \rightarrow \{[Co(HL)(OCOCH_3)_2(H_2O)_2] 2H_2O\}_n \quad (1)$$

$$Ni(CH_3COO)_2.4H_2O + HL \rightarrow \{[Ni(HL)(OCOCH_3)_2(H_2O)_2] 3H_2O\}_n \quad (2)$$

$$Mn(CH_3COO)_2.4H_2O + HL \rightarrow \{[Mn(HL)(OCOCH_3)_2(H_2O)_2] 2H_2O\}_n \quad (3)$$

$$Cd(CH_3COO)_2.2H_2O + HL \rightarrow \{[Cd(HL)_2(OCOCH_3)_2] 3H_2O\}_n \quad (4)$$

The general formulae of the polymeric complexes can be depicted as shown in (Figure 1). The C, H, N, S, and metal contents of polymer complexes gave satisfactory elemental analysis, suggesting 1:1/1:2 (metal: ligand) stoichiometry with the structure predicted (Figure 1). All the isolated polymer complexes are air stable for extended periods and remarkably soluble in DMSO and DMF.

3.2.2 | Molar conductance measurements

The conductance measurements recorded for 10^{-3} M solutions of the polymer complexes in DMSO are less polar. Very low molar conductance (Λ_M) values in the range of 8.44 to 20.33 ohm^{-1} cm^2 mol^{-1} in polymer complexes, that they are non-electrolytic. Hence the two acetate groups in the inside coordination sphere and confirmed by analytical data. The low Λ_M values may be attributed to the large cations.[1] The electrical conductivity of these polymer complexes found in order: Co(II) > Cd(II) > Ni(II) > Mn(II).
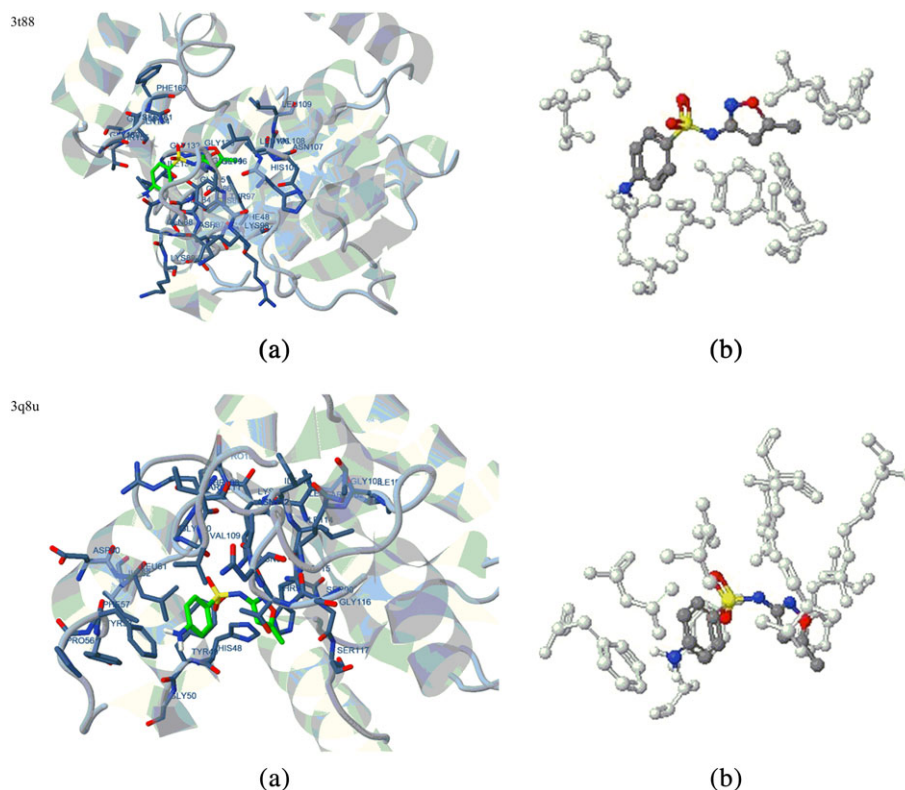
FIGURE 2 The start (green in (a) and gray in (b)) in interaction with receptors of crystal structures of *Escherichia coli* (3t88) and *Staphylococcus aureus* (3q8u)

3.3 | IR spectral studies

In the absence of a powerful technique such as X-ray crystallography. IR spectroscopy has proven to be the most suitable technique to give enough information to elucidate the nature of bonding of monomer to metal ion. The IR spectrum of monomer exhibits four potential donor sites, oxygen of the enolic (OH) group, nitrogen of isoxazole, sulphonamide (SO_2), and CONH groups (Figure 8). The CONH band nearly not changed indicating it is not involved in coordination. In the spectrum of monomer a broad band is observed in the region 3283-3178 cm^{-1}. This band attributed to $\upsilon(NH)$.

The IR data of the monomer and its polymer complexes are listed in Table 2. The IR spectra of the polymer complexes are compared with those of the monomer in order to determine the coordination sites that may involved in chelation. There are some guide peaks, in the spectra of the monomer, which are of good help for achieving this goal. The sharp peaks 1591 and 1518 cm^{-1} were due to the aromatic C=C stretching vibrations.[29] The absorption band at ~ 3283 cm^{-1}; $\upsilon(NH)$ of the sulphonamide group in the free monomer, was disappeared or hidden under the peak of water molecules. The presence of coordinated water molecules renders it difficult to confirm the enolization of the sulfonamide group. The SO_2 group modes of the monomer appear as

sharp bands at 1369 [$\upsilon_{asym}(SO_2)$] and 1162 [$\upsilon_{sym}(SO_2)$] cm^{-1}. In the polymer complexes, the asymmetric and symmetric modes are shifted, upon coordination to the transition metals.[30] The shift of the SO_2 stretching vibration to lower frequencies due to the transformation of the sulfonamide (-SO_2NH) to the enol form (-SO(OH)=N) as a result of complex formation to give more stable six-membered ring.[30] The band related to isoxazol ring stretching vibrations in the free monomer appeared at ~ 1473 cm^{-1} suffered a shift at 1481-1470 and 1412-1396 cm^{-1} in the spectra of polymer complexes indicating that the isoxazole moiety is participation in coordination.[31] In all the polymer complexes (1-3) the lattice/coordinated water molecules are indicated by the appearance of a broad band centered at ~3315-3403 cm^{-1}[24] as confirmed by thermal analysis. The rocking mode of coordination water is also observed in the range ~ 835 cm^{-1}.[24] It is assumed that the $\upsilon(NH)$ of CONH is merged with $\upsilon(OH)$ of coordinated water. The $\upsilon(C=O)$ of the CONH group is not changed. The coordination of acetate group is indicated by the appearance of two additional bands due to $\upsilon(COO^-)_{sym}$ and $\upsilon(COO^-)_{asym}$ at 1535-1523 and 1330-1311 cm^{-1}, respectively, in all the polymer complexes. The magnitude of $\Delta\upsilon$ = 205-212 cm^{-1} suggests the coordination of the acetate group in the unidentate fashion.[32] In the spectra of all polymer complexes, appearance of new bands in the region
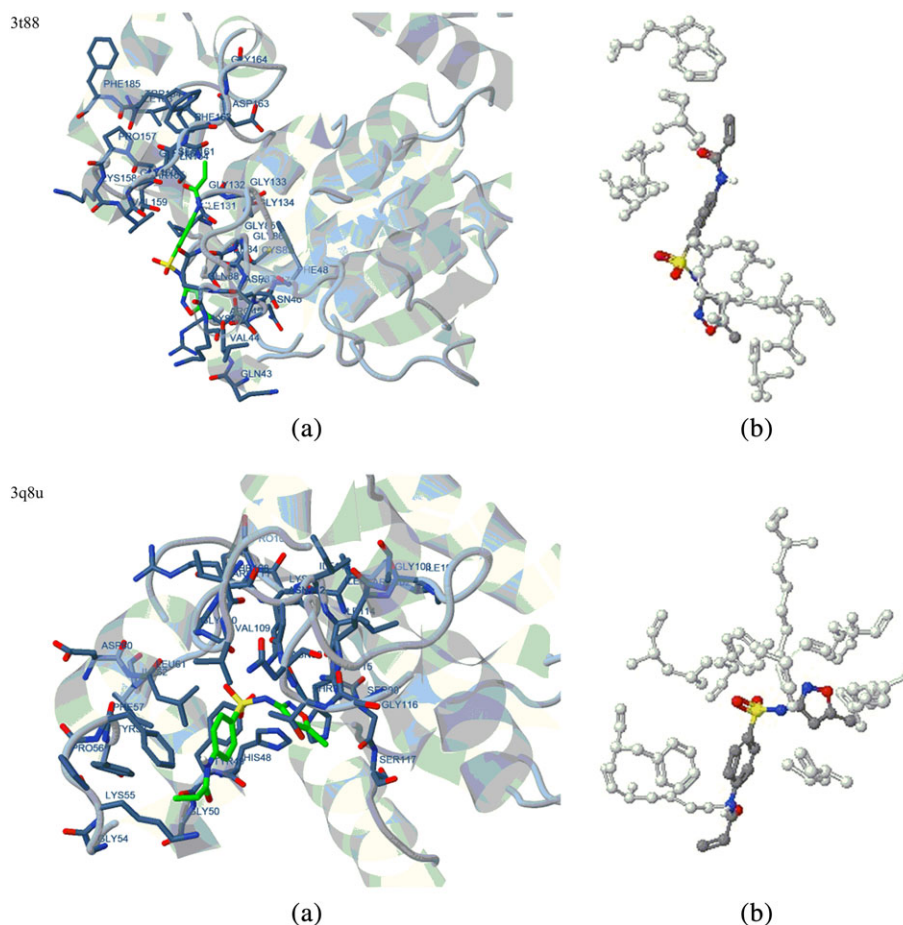
FIGURE 3 The HL (form A) (green in (a) and gray in (b)) in interaction with receptors of crystal structures of *Escherichia coli* (3t88) and *Staphylococcus aureus* (3q8u)

586-562 and 465-445 cm^{-1} has been attributed to M-O and M-N bonds, respectively.[33,34] From the IR spectral data it is concluded that monomer (HL) (form B) act as a bidentate ligand in polymer complexes, coordinating through enolic sulphonamide-OH and isoxazol-N moiety.

In ^{1}H NMR spectrum of monomer the absorption peaks at 10.64 - 11.25 ppm, assignable to hydrogen bonded NH or OH protons (Figure 1 and Figure 9a). These signals disappeared on repeating the measurements in the presence of D$_2$O (Figure 9b).

3.4 | Electronic spectra and magnetic measurements

The electronic spectrum of the free monomer exhibited two absorption bands at ~ 46500 cm^{-1} assigned to the π→π* transition for the intra-ligand of aromatic system C=C character and a strong band at ~ 37040 cm^{-1} is refer to n→π* transition for oxygen atom of S=O/C=O group or nitrogen atom of imine –N=C groups, respectively.[35] Upon complexation, there are some electronic changes

due to the interaction of monomer with Ni(II), Co(II) and Mn(II) metal ions.

The electronic spectrum of Ni(II) polymer complex exhibits bands at 10800 cm^{-1} [^{3}A$_{2g}$ → ^{3}T$_{2g}$(F)(υ$_1$)], 17200 cm^{-1} [^{3}A$_{2g}$ → ^{3}T$_{1g}$(F)(υ$_2$)] and 263000 cm^{-1} [^{3}A$_{2g}$ → ^{3}T$_{1g}$(P)(υ$_3$)] transitions in an octahedral field. [36] The υ$_2$/υ$_1$ ratio is 1.59 which occurs in the usual range (1.60-1.82) expected for octahedral Ni(II) complexes. [24] The spectral parameters of the Ni(II) polymer complex as calculated according to the method of Lever [37] are as follows: Dq = 1080 cm^{-1}, B^o = 740 cm^{-1}, β = 0.71 and LFSE (kcal mol^{-1}) = 37.12. The reduction of the Racah parameter from the free ion value of 1038 cm^{-1} and the β^o = 29% are indicative of the presence of strong covalency in the polymer complex.

Co(II) polymer complex exhibits absorption bands at 9010 cm^{-1} [^{4}T$_{1g}$(F) → ^{4}T$_{2g}$(F)(υ$_1$)], 18350 cm^{-1} [^{4}T$_{1g}$(F) → ^{4}A$_{2g}$(F)(υ$_2$)] and 21250 cm^{-1} [^{4}T$_{1g}$(F) → ^{4}T$_{1g}$(P)(υ$_3$)] transitions, and the magnetic moment for the Co(II) polymer complex in the 4.80 B.M. supporting octahedral geometry.[38] The ligand field splitting energy (10Dq = 9340 cm^{-1}), interelectronic repulsion parameters (B^o =
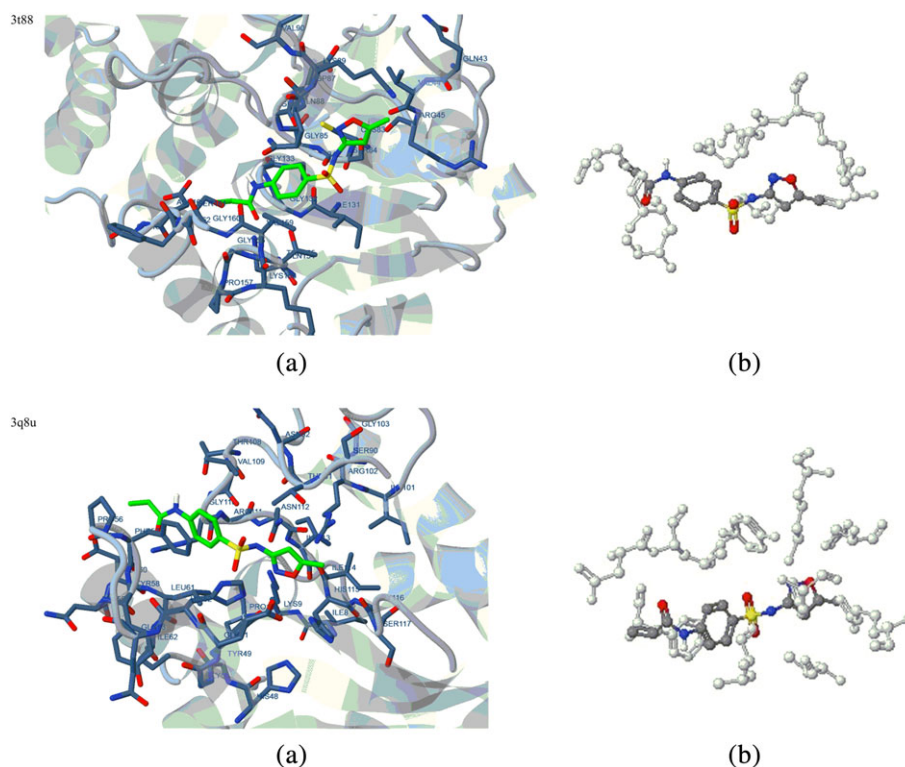
FIGURE 4 The HL (form B) (green in (a) and gray in (b)) in interaction with receptors of crystal structures of *Escherichia coli* (3t88) and *Staphylococcus aureus* (3q8u)

TABLE 1 Energy values obtained in docking calculations of start and HL (form A and form B) with receptors of crystal structures of *Escherichia coli* (3t88) and *Staphylococcus aureus* (3q8u)

| Compound[a]	Receptors	Est. Free Energy of Binding (kcal/mol)	Est. inhibition constant (K_i) (µM)	vdW+ bond+ desolv energy (kcal/mol)	Electrostatic Energy (kcal/mol)	Total intercooled Energy (kcal/mol)	Interact surface
Start	3 t88	-4.27	743.12	-5.15	-0.20	-5.35	560.196
	3q8u	-5.41	107.62	-5.46	-0.90	-6.36	627.268
HL (form A)	3 t88	-5.04	202.19	-5.88	-0.88	-6.77	574.327
	3q8u	-5.50	93.57	-6.22	-0.76	-6.97	725.422
HL (form B)	3 t88	-5.11	178.63	-6.63	-0.04	-6.67	701.529
	3q8u	-5.79	56.78	-7.24	-0.10	-7.34	759.070

[a]Symbols as given in Figure 1.

838 cm^{-1}) and covalency factor (nephelauxetic ratio) (β = 0.75) and LFSE (kcal mol^{-1}) = 26.75 for the octahedral Co(II) polymer complexes have been calculated using the secular equation given by Konig.[39] The υ_2/υ_1 ratio is 2.04 which occurs in the usual range expected for octahedral Co(II) complexes.

Mn(II) polymer complex shows four electronic absorption bands at 19602 cm^{-1} [$^6A_{1g} \rightarrow {}^4T_{2g}(G)$], 23805 cm^{-1} [$^6A_{1g} \rightarrow {}^4Eg, {}^4A_{1g}(^4G)$] (10B + 5C), 28568 cm^{-1} [$^6A_{1g} \rightarrow {}^4Eg(^4G)$] (17B = 5C) and 29846 cm^{-1} [$6A_{1g} \rightarrow {}^4T_{1g}(^4P)$] transitions, suggesting of octahedral geometry.[37] Mn(II) polymer complex in the present study show magnetic

moment is 5.91 B.M., indicating the presence of five unpaired spins and hence there is high-spin complex.

The experimentally observed transition energies are used to calculate the values of parameters B, C, Dq and β. Various ligand field parameters were calculated for the polymer complexes and the value of Dq in Co(II) polymer complex was calculated from transition energy [40] and in Ni(II) and Mn(II) Dq obtained from the first transition. The Naphelauxetic (β) was readily obtained by using the relation β = B(complex)/B(free ion). The values of β lie in the range of 0.87-0.75. Parameters B and C are linear combinations of certain coulomb's and exchange
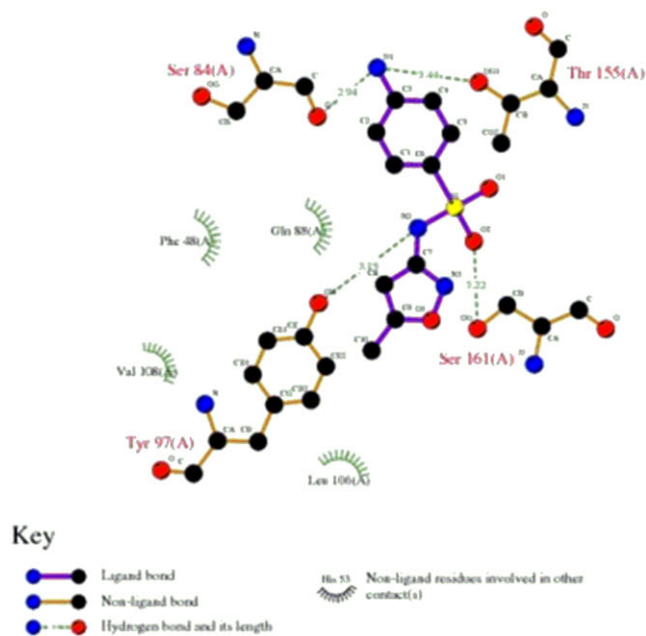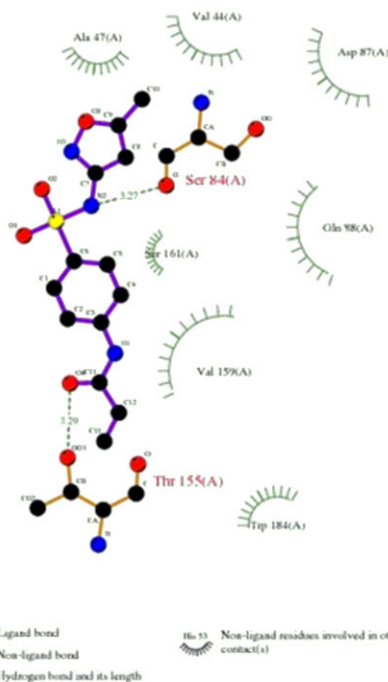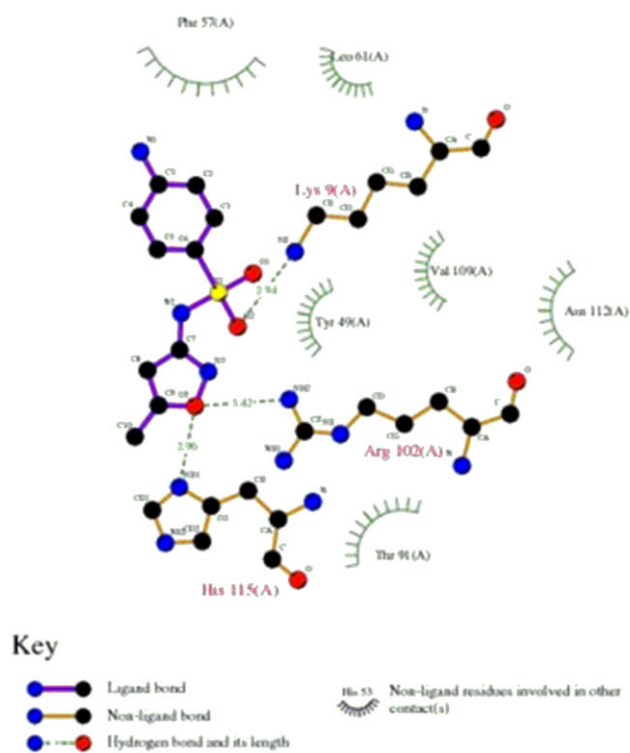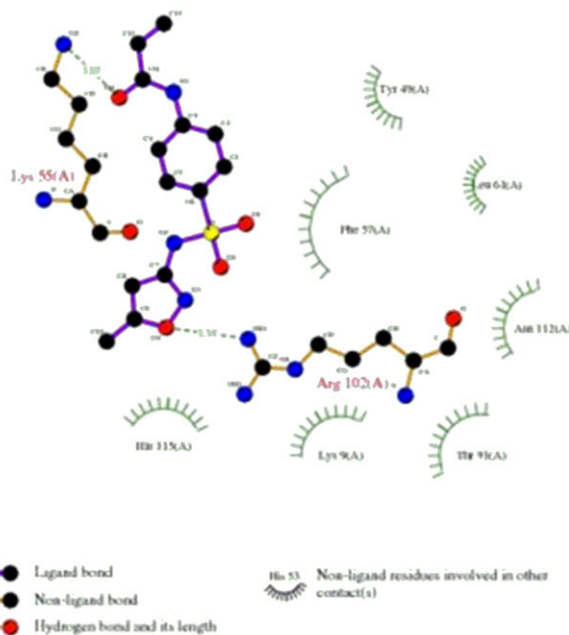
FIGURE 5 2D plot of interaction between start and receptors (a) crystal structure of *Escherichia coli* (3t88) and (b) crystal structure of *Staphylococcus aureus* (3q8u)

FIGURE 6 2D plot of interaction between HL (form A) and receptors (a) crystal structure of *Escherichia coli* (3t88) and (b) crystal structure of *Staphylococcus aureus* (3q8u)

integral and are generally treated as empirical parameters obtained from the spectra of the free ion. Slater Condon-Shortly parameters F_2 and F_4 are related to the Racah inter-electronic repulsion parameters B and C. By using values of the Racah parameters B and C values for the parameters B (680 cm^{-1}) and C (3401 cm^{-1}), values for the parameters F_2 (1166) and F_4 (97) have been calculated. The electron-electron repulsion in the complex is less than

Key

- Ligand bond
- Non-ligand bond
- Hydrogen bond and its length

His 53 Non-ligand residues involved in other contact(s)

docking

(a)

Key

- Ligand bond
- Non-ligand bond
- Hydrogen bond and its length

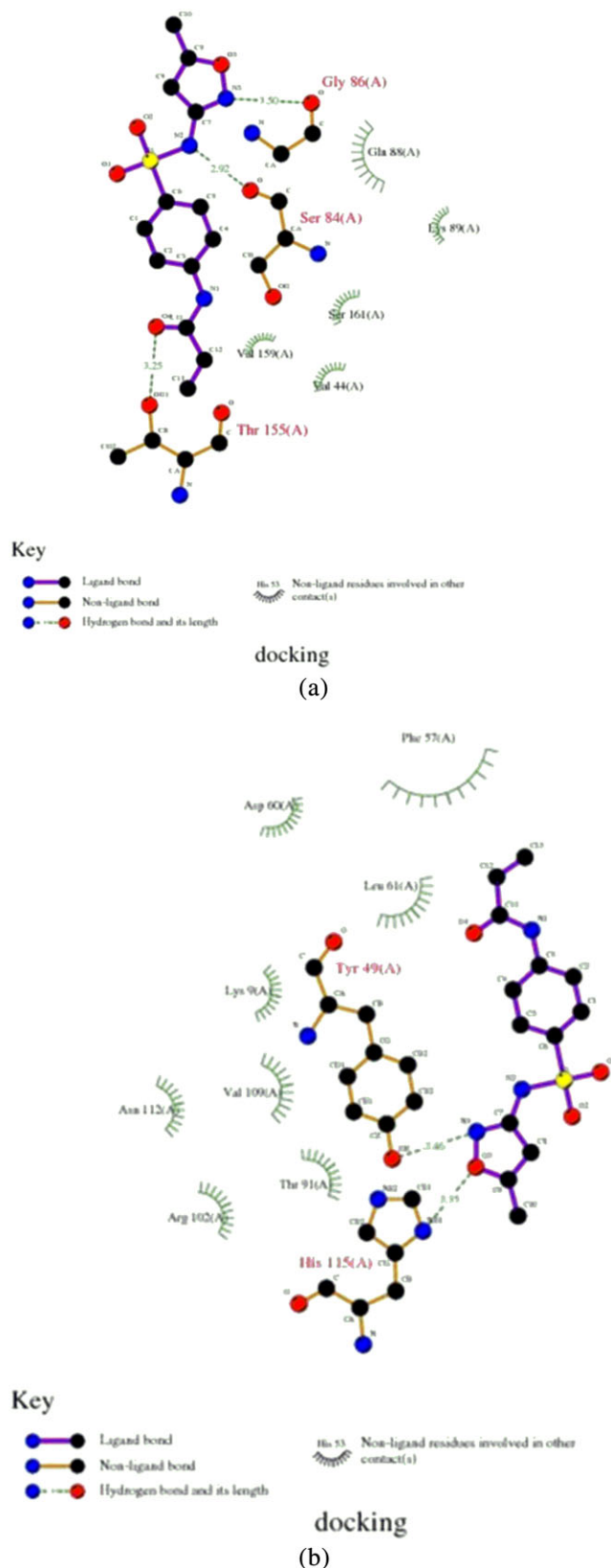His 53 Non-ligand residues involved in other contact(s)

docking

(b)

FIGURE 7 2D plot of interaction between HL (form B) and receptors (a) crystal structure of *Escherichia coli* (3t88) and (b) crystal structure of *Staphylococcus aureus* (3q8u)

the free ion, resulting the increased distance between electrons and thus, an effective increase in the size of the orbital will take place. On increasing delocalization, the value of β (0.87) decreases. This is why the calculated value of the β in the present complex is less than one. This indicates that the complex under study has appreciable covalent character in metal ligand (M-L) bond.

3.5 | X-ray diffraction analysis

The X-ray diffraction (XRD) patterns powder forms of monomer and polymer complexes **(1, 3** and **4)** are shown in Figure 10. The XRD patterns of polymer complexes **(1, 3** and **4)** show a broad peak in the range of $2\theta^o = 20\text{-} 27^o$ indicating a completely amorphous structures while monomer shows many diffraction peaks which indicate the polycrystalline phase.[41]

3.6 | Thermal analysis of HL and its polymer complexes

The thermal properties of HL and its metal polymer complexes were characterized on the basis of thermogravimetric analysis (TGA) method in the temperature range 30–800 °C (Figure 11). The effect of temperature and the percentage of loss of mass are listed in Table 3. The TGA curve of the HL show three composition steps, the first step is at temperature range 50–163 °C and it suits loss of CH_3 (found 4.84%; calc. 4.89%) and the second stage at the temperature range 163-426 °C suits to loss of $C_3H_2N_2SO$ (found 37.12%; calc. 37.13%). The final stage at the temperature range 426-800 °C suits to loss of $C_9H_8NO_3$ (found 58.04%; calc. 57.98%).

Complex $\{[Co(HL)(OCOCH_3)_2(H_2O)_2]\ 2H_2O\}_n$ **(1)** decomposed at three stages, the first stage at temperature range 25–76 °C which related to evaluation of $2H_2O$ molecules (found 6.71%; calc. 6.48%).[42] The second stage in the range 76-456 °C correlated with the loss of $2H_2O + 2CH_3COO + C_9H_9N_2O_3S$ (found 67.60%; calc. 66.02%). The third stage in the range 456-726 °C, the complex loss C_3H_4N (found 9.60 %; calc. 9.71%) and one carbon atom and CoO remained as a final product (found 16.09 %; calc. 15.64%).

Complex $\{[Ni(HL)(OCOCH_3)_2(H_2O)_2]\ 3H_2O\}_n$ **(2)** decomposed at three stages, the first stage at temperature range 30-93 °C which correspond to loss $3H_2O$ molecules (found 9.61%; calc. 9.41%). The second stage in the range 93-428 °C which related to loss a part of $2H_2O + 2CH_3COO + C_8H_8NO$ (found 49.13%; calc. 50.20%), the third stage in the range 428-800 °C the complex loss $C_4H_5N_2O_2S$ (found 25.60%; calc. 25.28%) and leaving one carbon atom and NiO as a final product (found 15.66%; calc. 15.11%).

Complex $\{[Mn(HL)(OCOCH_3)_2(H_2O)_2]\ 2H_2O\}_n$ **(3)** decomposed at three stages, the first stage at
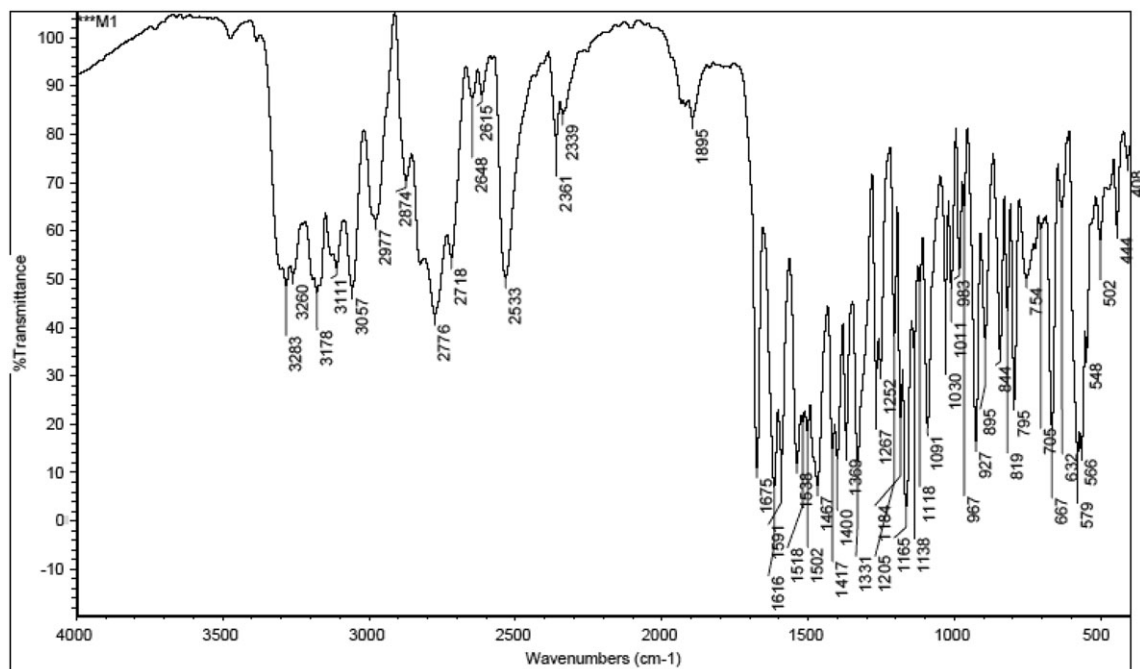
FIGURE 8 IR spectrum of monomer

TABLE 2 IR spectra (cm^{-1}) of the monomer and its polymer complexes

Compound	υ(NH)	υ(OH) enolic	υ(SO$_2$) (asym)	υ(SO$_2$) (sym.)	υ(H$_2$O) (coord)	Isoxazole Ring str.	υ(M-O)	υ(M-N)
HL	3283,3260, 3178	-	1337	1156	-	1467,1417, 1369	-	-
{[Co(HL)(OCOCH$_3$)$_2$(H$_2$O)$_2$] 2H$_2$O}$_n$ **(1)**	-	3060	1311	1162	835,794	1475,1412	592	440
{[Ni(HL)(OCOCH$_3$)$_2$(H$_2$O)$_2$] 3H$_2$O}$_n$ **(2)**	-	3080	1307	1132	835,764	1481,1411	594	445
{[Mn(HL)(OCOCH$_3$)$_2$(H$_2$O)$_2$] 2H$_2$O}$_n$ **(3)**	-	3108	1330	1162	835,796	1470,1396	569	480
{[Cd(HL)$_2$(OCOCH$_3$)$_2$] 3H$_2$O}$_n$ **(4)**	-	3112	1313	1164	-	1473,1404	586	435

temperature range 30-95 °C which correspond to loss 2H$_2$O molecules (found 5.85%; calc. 6.52%) and the second stage in the range 95-455 °C which related to loss a part of 2H$_2$O + 2CH$_3$COO (found 27.19%; calc. 27.90%). The third stage in the range 455-780 °C the complex loss C$_8$H$_{13}$N$_3$SO$_3$ (found 42.51%; calc. 41.84%) and five carbon atoms and MnO remained as residue (found 25.45%; calc. 23.93%).

Complex {[Cd(HL)$_2$(OCOCH$_3$)$_2$] 3H$_2$O}$_n$ **(4)** decomposed at four stages, the first stage at temperature range 35-112 °C related to evaluation of 3H$_2$O molecules (found 6.13%; calc. 6.01%). The second stage in the range 112-240 °C related to evaluation of CH$_3$COO (found 6.59%; calc. 6.57%) and the third stage in the range 240-470 °C which correlated with elimination a part of CH$_3$COO + C$_6$H$_{10}$N$_4$S$_2$O$_5$ (found 37.34%; calc. 37.96%). The fourth stage, which was the final stage, in the range 470-800 °C loss C$_{20}$H$_{16}$N$_2$O$_2$ (found 35.04%; calc. 35.17%) and leaving CdO as a final product (found 14.90%; calc. 14.29%).

3.7 | Kinetic studies

The kinetic parameters such as the thermal activation energy of decomposition (E$_a$), enthalpy (ΔH^*), entropy (ΔS^*) and Gibbs free energy change of the decomposition (ΔG^*) are evaluated graphically by employing the Coast-Redfern and Horowitz-Metzger methods.[43,44]

3.7.1 | Coast-Redfern equation

The Coast-Redfern equation, which is a typical integral method, can represent as:

$$\int_0^a \frac{dx}{(1-\alpha)^n} = \frac{A}{\phi}\int_{T_1}^{T_2} \exp\left(-\frac{E_a}{RT}\right)dt \qquad (5)$$

For convenience of integration, the lower limit T$_1$ usually taken as zero. This equation on integration gives:

$$\ln\left[-\frac{\ln(1-\alpha)}{T^2}\right] = -\frac{E_a}{RT} + \ln\left[\frac{AR}{\varphi E_a}\right] \qquad (6)$$

(a)

(b)
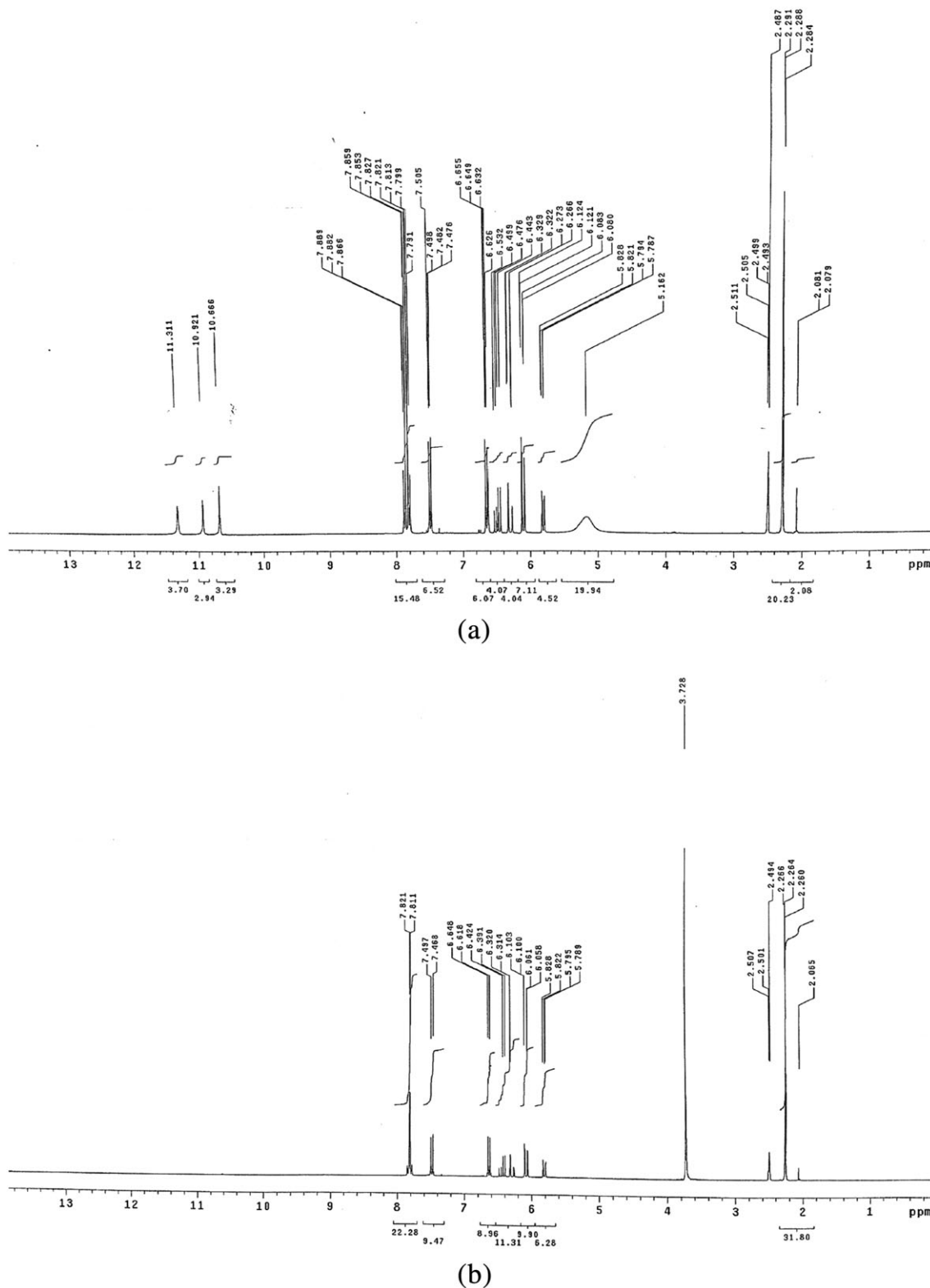
FIGURE 9 ¹H-NMR spectrum of (a) monomer and (b) monomer with D_2O

A plot of left-hand side (LHS) against 1/T was drawn (Figure 12). E_a is the energy of activation and calculated from the slop. The entropy of activation calculated by using the equation:

$$\Delta S^* = 2.303 \left[\log \left(\frac{Ah}{k_B T_s} \right) \right] R \qquad (7)$$

where k_B is the Boltzmann constant, h is the Plank's constant and T_s is the TG peak temperature.

FIGURE 11 TGA curves of HL and polymer complexes

3.7.2 | Horowitz-Metzger equation

The Horowitz-Metzger equation is an illustrative of the approximation methods. These authors derived the relation:

$$\log\left[\frac{1-(1-\alpha)^{1-n}}{1-n}\right] = \frac{E_a\theta}{2.303RT_s^2}, \quad \text{for } n\neq1 \quad (8)$$
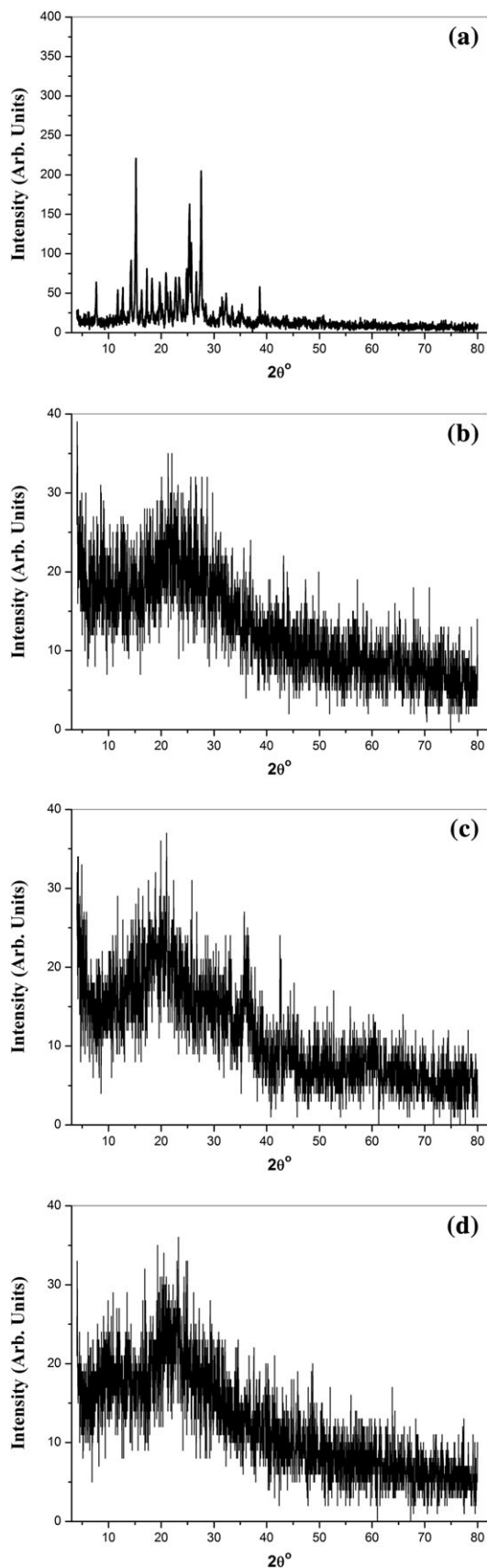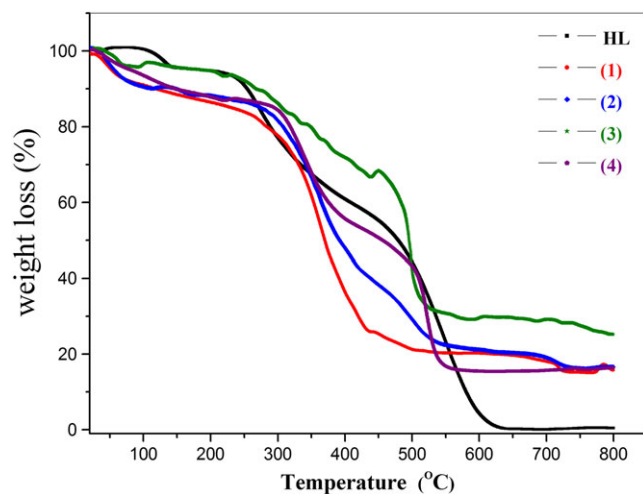
when n = 1, the LHS of equation 8 would be log[-log(1-α)] (Figure 13). For a first order kinetic process, the Horowitz-Metzger equation may write in the form:

$$\log\left[\log\left(\frac{W_\alpha}{W\gamma}\right)\right] = \frac{E_a\theta}{2.303RT_s^2} - \log 2.303 \quad (9)$$

where $\theta = T-T_s$, $w_\gamma = w_\alpha - w$, w_α = mass loss at the completion reaction; w = mass loss up to time t. The plot of log [log (w_α/w_γ)] vs. θ was drawn and found to be linear from the slope of which E_a was calculated. The pre-exponential factor, A, calculated from equation:

$$E_a/RT_s^2 = A/\left[\varphi\exp\left(-\frac{E_a}{RT_s}\right)\right] \quad (10)$$

The entropy of activation, ΔS^*, is calculated from equation 7. The enthalpy activation, ΔH^*, and Gibbs free energy, ΔG^*, calculated from:

$$\Delta H^* = E_a - RT \quad (11)$$

$$\Delta G^* = \Delta H^* - T\,\Delta S^* \quad (12)$$

The calculated values of E_a, A, ΔS^*, ΔH^* and ΔG^* for the decomposition steps for HL monomer and its polymer complexes **(1-4)** are summarized in Table 4. The kinetic data obtained from the two methods are comparable and

FIGURE 10 X-ray diffraction patterns of powder forms for a) monomer, b) polymer complex **(1)**, c) polymer complex **(3)** and d) polymer complex **(4)**

TABLE 3 TGA analyses of monomer and polymer complexes

Compound[a]	TG range (°C)	Mass loss Found (Calcd.) %	Assignment
HL	50–163	4.84 (4.89)	CH_3
	163-426	37.12 (37.13)	$C_3H_2N_2SO$
	426-800	58.04 (57.98)	$C_9H_8NO_3$
(1)	25–76	6.71 (6.48)	$2H_2O$
	76-456	67.60 (66.02)	$2H_2O + 2CH_3COO + C_9H_9N_2O_3S$
	456-726	9.60 (9.71)	C_3H_4N
	< 726	16.09 (15.64)	$CoO + C$
(2)	30-93	9.61 (9.41)	$3H_2O$
	93-428	49.13 (50.20)	$2H_2O + 2CH_3COO + C_8H_8NO$
	428-800	25.60 (25.28)	$C_4H_5N_2O_2S$
	< 800	15.66 (15.11)	$NiO + C$
(3)	30-95	5.85 (6.52)	$2H_2O$
	95-455	27.19 (27.90)	$2H_2O + 2CH_3COO$
	455-780	42.51 (41.84)	$C_8H_{13}N_3SO_3$
	< 780	25.45 (23.93)	$MnO + 5C$
(4)	35-112	6.13 (6.01)	$3H_2O$
	112-240	6.59 (6.57)	CH_3COO
	240-470	37.34 (37.96)	$CH_3COO + C_6H_{10}N_4S_2O_5$
	470-800	35.04 (35.17)	$C_{20}H_{16}N_2O_2$
	< 800	14.90 (14.29)	CdO

[a]Numbers as given in Table 2.

can be considered in good agreement with each other.[24,45] From the values of the thermal activation energy of decomposition (E_a) of HL monomer and its polymer complexes (1-4), it was found that the E_a value for the complex (1) is higher compared to the other complexes.

The entropy is found to be negative values in the HL and its polymer complexes (1-4) which indicates more ordered activated complex than the reactants or the reaction is slow.[38] The positive value of ΔG^* for HL and its polymer complexes (1-4) is non-spontaneous processes.

3.8 | Antimicrobial activity studies

Antimicrobial activities of sulphadrugs and metal complexes may be enhanced by the presence of oxygen, nitrogen, and sulfur atoms which have chelating properties.[46] Antibacterial and antifungal activities of monomer and metal polymer complexes were tested against three local Gram positive bacteria (*Bacillus cereus*, *Staphylococcus aureus* and *Enterococcus faecalis*), three local Gram negative bacteria (*Escherichia coli*, *Klebsiella pneumoniae* and *Pseudomonas aeruginosa*) and three local fungi (*Aspergillus niger*, *Fusarium oxysporum* and the yeast *Candida albicans*) and the results were recorded in Tables 5 and 6. All the monomer and polymer complexes have no antibacterial activity against Gram positive bacteria and Gram negative bacteria except Cd(II) polymer complex (4) has antibacterial activity against *Staphylococcus aureus*,

Escherichia coli and *Klebsiella pneumoniae* (Table 5). It was found that Cd(II) polymer complex (4) has more antibacterial activity than the penicillin against *Klebsiella pneumoniae*. The activity of the Cd(II) polymer complex (4) may be due the fact that:

1. Cd(II) polymer complex (4) has corresponding metal chloride salt in 1:2 (metal: monomer) molar ratio (Section 2).
2. the Cd(II) polymer complex (4) has more than one unit of sulfonamide. [46]

The antifungal activity results of the HL and its polymer complexes were investigated against *Aspergillus niger*, *Fusarium oxysporum* and the yeast *Candida albicans* and listed in Table 6. It was found that the monomer and M(II) complexes polymer have neither antifungal nor anticandidal activities.

3.9 | DNA binding activity study

DNA binding usually exhibits hypochromic as a consequence of the intercalation mode, which involves a strong stacking interaction between an aromatic chromophore and the base pairs of DNA. The intrinsic binding constant to CT-DNA by monitoring the absorption intensity of the charge transfer spectral bands near 262 nm for the HL and 259, 256, 259 and 259 nm for polymer complexes (1-4), respectively, was determined.
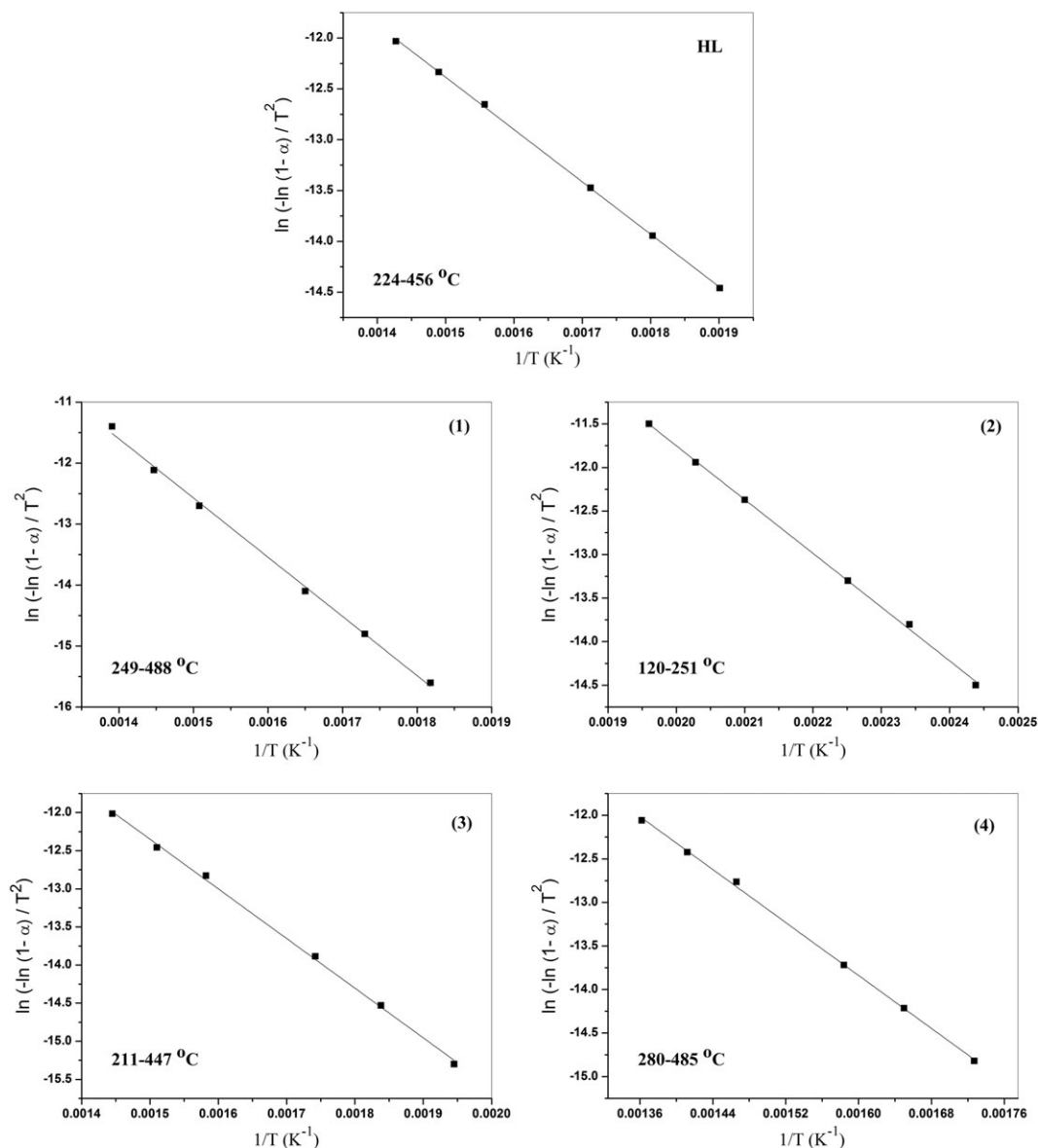
FIGURE 12   Coats–Redfern (CR) of HL and its polymer complexes

DNA interaction study by UV–Visible spectroscopy electronic absorption spectra was initially used to examine the interaction between ligand and CT-DNA. After interaction with increasing amount of DNA, the absorption spectra of HL monomer and its polymer complexes **(1-4)** display clear hypochromism with slight red shift (~1-2 nm). These interactions result in the observed hypochromic [28,38]. The intrinsic binding constant (K_b) values obtained from the absorption spectral technique (Figure 14) were calculated as 2.19 $\times 10^5$ M^{-1} for HL and 8.62 $\times 10^5$ M^{-1}, 1.16 $\times 10^6$ M^{-1}, 6.51 $\times 10^5$ M^{-1} and 2.91 $\times 10^5$ M^{-1} for polymer complexes **(1-4)**, respectively. From these results we noted that the highest value of K_b is belong complex **(2)** and these indicated that the Ni(II) is highly binding with CT-DNA and these due to the lower ionic radiusas shown in Figure 15.

3.10 | Corrosion inhibition of C38 steel using HL

3.10.1 | Potentiodynamic polarization measurement

Polarization tests were done in order to gain knowledge concerning the kinetics of the cathodic and anodic reactions. Figure 16 shows the polarization behavior of C38 steel electrode in 2 M HCl without and with unlike dose of HL. Figure 16 gives that both the cathodic and anodic reactions are impressive by the putting of

TABLE 4 Thermodynamic parameters for monomer and polymer complexes

| Compound[a]	Temp. range (°C)	Method	Parameter				Correlation coefficient (r)
			E_a (kJ mol^{-1})	ΔS^* (J mol^{-1} K^{-1})	ΔH^* (kJ mol^{-1})	ΔG^* (kJ mol^{-1})	
HL	224-456	CR	42.8	-2.34E+02	37.7	181	0.99967
		HM	50.5	-2.18E+02	45.4	179	0.99894
(1)	249-448	CR	80.7	-1.73E+02	75.5	185	0.99745
		HM	92.4	-1.51E+02	87.1	183	0.99805
(2)	120-251	CR	51.3	-1.86E+02	47.5	133	0.99941
		HM	57.7	-1.66E+02	53.9	130	0.9984
(3)	211-447	CR	54.2	-2.14E+02	49.2	178	0.99849
		HM	63.9	-1.92E+02	58.9	174	0.99848
(4)	280-485	CR	63.2	-2.06E+02	57.7	193	0.99907
		HM	73	-1.87E+02	67.6	191	0.99823

[a]Numbers as given in Table 2.
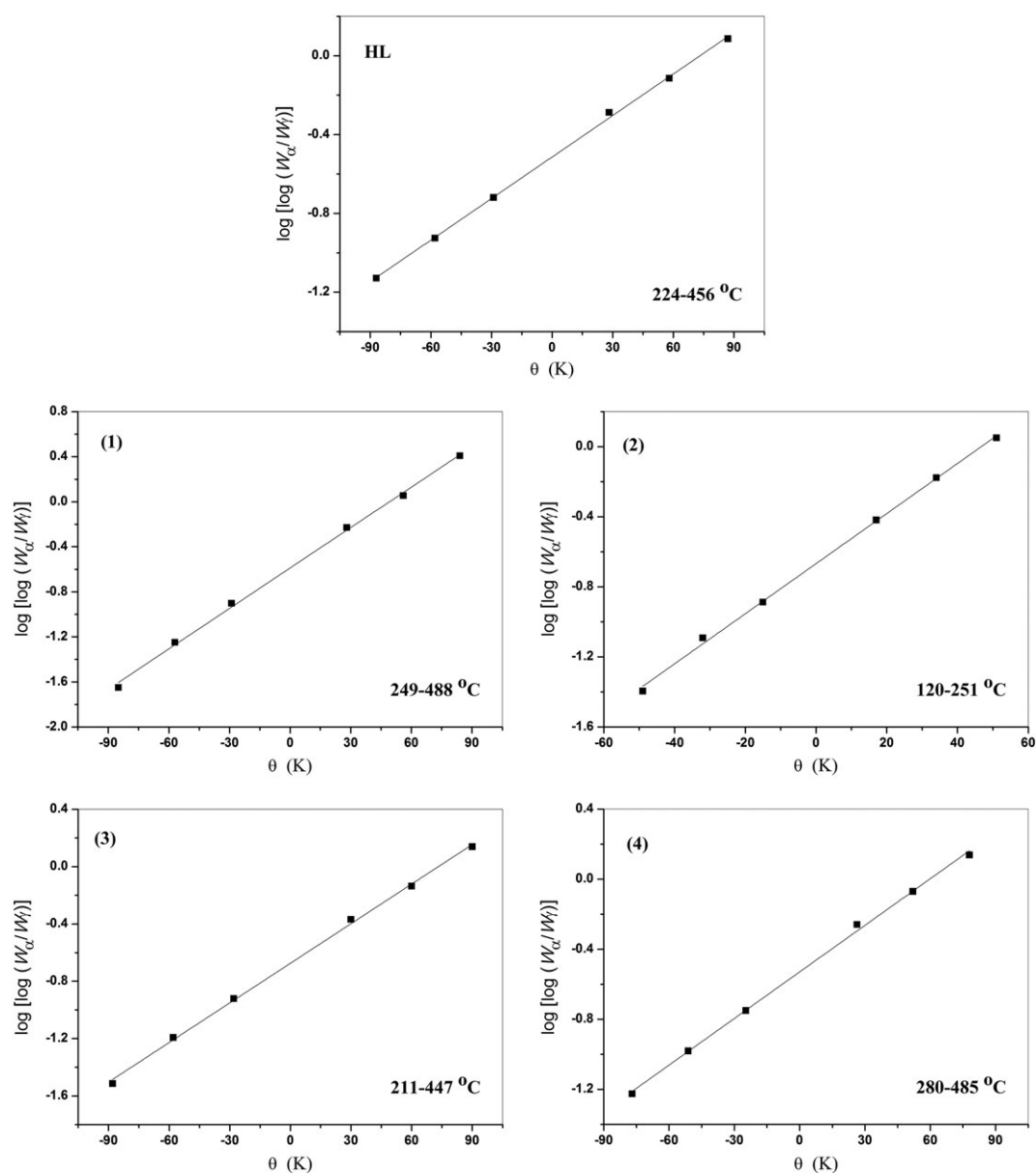
FIGURE 13 Horowitz–Metzger (HM) of HL and its polymer complexes

TABLE 5 Antibacterial activity data of monomer and polymer complexes. The results were recorded as the average diameter of inhibition zone (mm) ± standard deviation

Compound[a]	Conc. (μg/ml)	Gram positive bacteria			Gram negative bacteria		
		Bacillus cereus	*Staphylococcus aureus*	*Enterococcus faecalis*	*Escherichia coli*	*Klebsiella pneumoniae*	*Pseudomonas aeruginosa*
HL	50	-ve	-ve	-ve	-ve	-ve	-ve
	100	-ve	-ve	-ve	-ve	-ve	-ve
	150	-ve	-ve	-ve	0.3 ± 0	-ve	-ve
(1)	50	-ve	-ve	-ve	-ve	-ve	-ve
	100	-ve	-ve	-ve	-ve	-ve	-ve
	150	-ve	-ve	-ve	-ve	-ve	-ve
(2)	50	-ve	-ve	-ve	-ve	-ve	-ve
	100	-ve	-ve	-ve	-ve	-ve	-ve
	150	-ve	-ve	-ve	-ve	-ve	-ve
(3)	50	-ve	-ve	-ve	-ve	-ve	-ve
	100	-ve	-ve	-ve	-ve	-ve	-ve
	150	-ve	-ve	-ve	-ve	-ve	-ve
(4)	50	-ve	0.2 ± 0	-ve	0.4 ± 0	0.4 ± 0*	-ve
	100	-ve	0.2 ± 0	-ve	0.8 ± 0	0.55 ± 0.04*	-ve
	150	-ve	0.2 ± 0	-ve	0.8 ± 0	0.60 ± 0*	-ve
Penicillin	50	1 ± 0.14	2 ± 0	1.46 ± 0.03	1 ± 0	-ve	0.87 ± 0.033
	100	3 ± 0.28	2 ± 0.14	1.86 ± 0.03	3 ± 0	-ve	1.06 ± 0.033
	150	3 ± 0.14	2 ± 0	2.2 ± 0	3 ± 0	-ve	1.4 ± 0.058

[a]Numbers as given in Table 2.

*Indicate significant different value from that of penicillin.

TABLE 6 Antifungal activity data of monomer and polymer complexes. The results were recorded as the average diameter of inhibition zone (mm) ± standard deviation

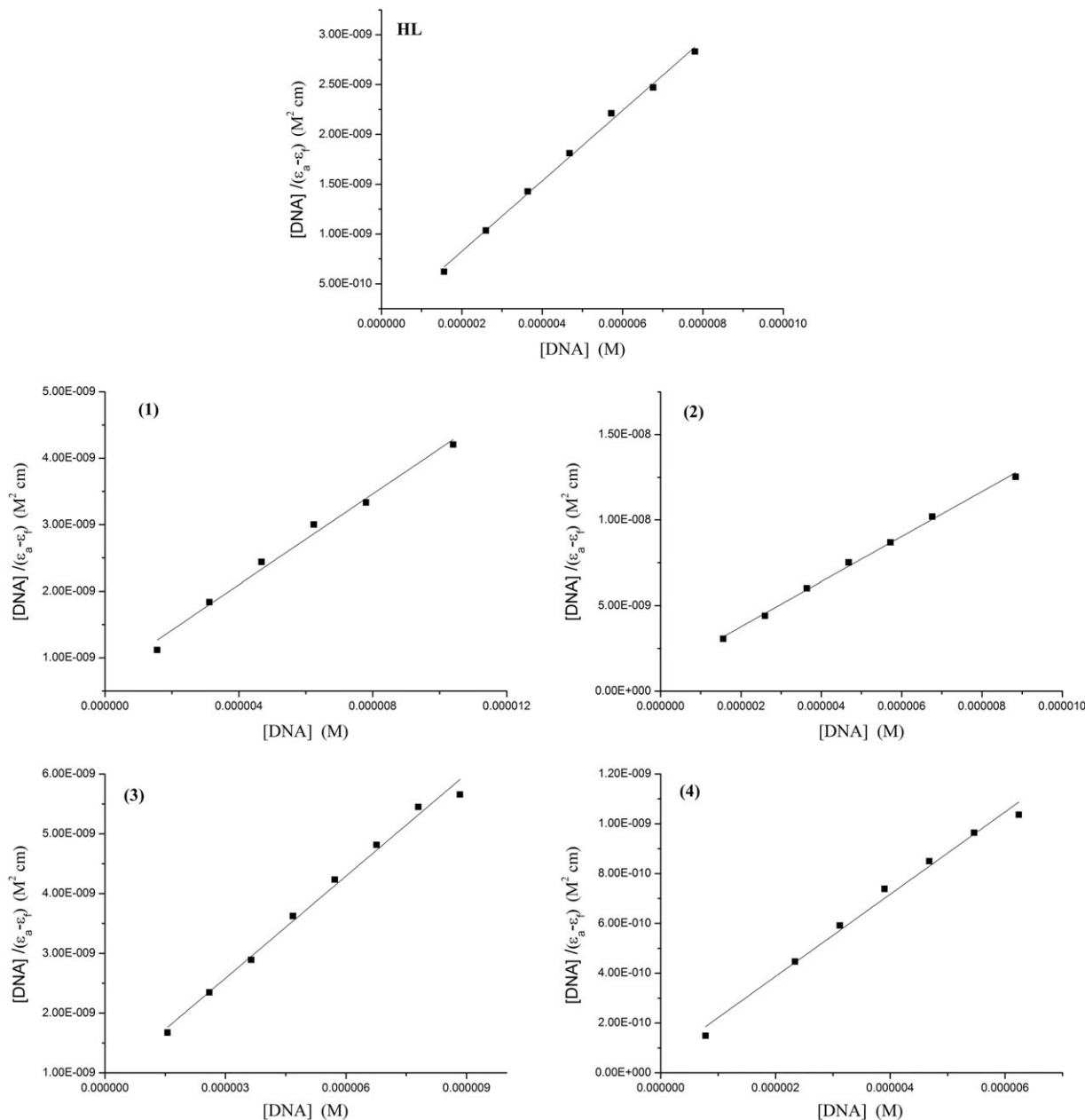| Compound[a]	Conc. (μg/ml)	*Aspergillus niger*	*Fusarium oxysporum*	*Candida albicans*
HL	50	-ve	-ve	-ve
	100	-ve	-ve	-ve
	150	-ve	-ve	-ve
(1)	50	-ve	-ve	-ve
	100	-ve	-ve	-ve
	150	-ve	-ve	-ve
(2)	50	-ve	-ve	-ve
	100	-ve	-ve	-ve
	150	-ve	-ve	-ve
(3)	50	-ve	-ve	-ve
	100	-ve	-ve	-ve
	150	-ve	-ve	-ve
(4)	50	-ve	-ve	-ve
	100	-ve	-ve	-ve
	150	-ve	-ve	-ve
Miconazole	50	1 ± 0	2 ± 0	1.1 ± 0
	100	3 ± 0.14	3 ± 0	1.3 ± 0
	150	4 ± 0	3 ± 0	1.7 ± 0.058

[a]Numbers as given in Table 2.

FIGURE 14 Plot of [DNA]/($\varepsilon_a - \varepsilon_f$) as function of DNA concentration as determined from the absorption spectral data of HL and its polymer complexes

investigated HL and the protection efficiency improve as the inhibitor dose rise, but the cathodic reaction is more inhibited, i.e the addition HL lower the anodic liquefaction of alloy and also prevent the cathodic reactions. Therefore, HL is play as mixed kind inhibitor.

The data in Table 7 given corrosion current density lower obviously after the appending of inhibitors in 2 molar acid and % IE rise with higher the dose of inhibitor. The E_{corr} with inhibitor was improve with no definite trend, lead to that this inhibitor play as mixed–kind inhibitors. %IE$_p$ was record by utilized equation:

$$\%IE_p = [\ i^o_{corr} - i_{corr})/i^o_{corr}]x\ 100 \qquad (13)$$

where i_{corr} and i^o_{corr} are the inhibited and lack inhibited current corrosion densities, respectively.

It is evident from Table 7 that the (β_a) and (β_c) Tafel lines equal upon unchanged appending of organic derivatives, improvement to a nearly parallel set of anodic lines, and almost parallel cathodic curves record too. The inhibitor adsorbed lower the surface area for corrosion without impressive of the mechanism corrosion of alloy in acidic solution.[47]
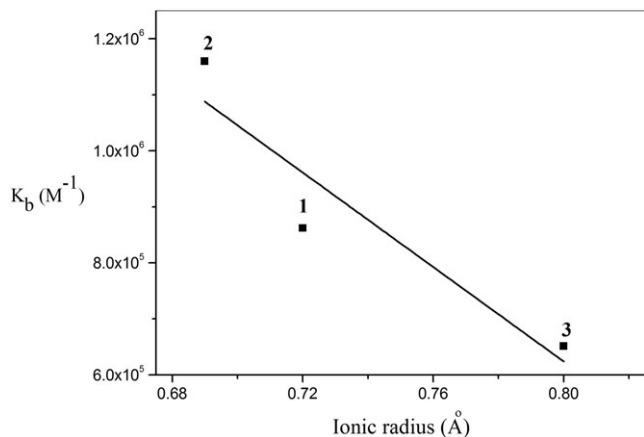
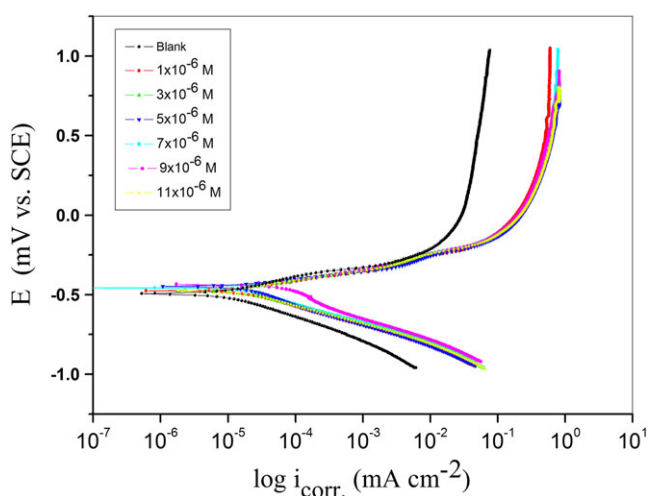**FIGURE 15** The relation between ionic radius of metal complexes *vs.* intrinsic binding constants (K_b)

FIGURE 16 Tafel polarization diagrams for the corrosion of C38 steel in 2 M hydrochloric acid attendance and lack of unlike dose of HL at 30 ± 1 °C

3.10.2 | EIS test

EIS is a powerful method in the research of corrosion. Mechanistic information, properties of surface and kinetics of electrode can be given from impedance plots.[38]

Figure 17 given Nyquist (a) and Bode (b) curves given at open-circuit potential both in lack and attendance of rising dose of investigated HL. The improvement in the size of the capacitive loop with the appending of HL gives that a gradually barrier forms on the alloy surface. The rise in the size of capacitive loop Figure 17(a) enhances, at a fixed inhibitor dose.

The Nyquist digrames do not given best semicircles as theory expected of EIS. The change from ideal semicircle due to the dispersion of frequency as well as to the inhomogeneity's of the surface. The C_{dl} (double layer capacitance) is measured from equation 14:

$$C_{dl} = Y_o \omega^{n-1} / \sin [n (\pi/2)] \qquad (14)$$

where Y_o = CPE magnitude, $\omega = 2\pi f_{max}$, f_{max} = the imaginary frequency at which the component of the impedance is maximal.

After test the shape of the Nyquist curves, the corrosion process was controlled mainly charged-transfer.[47] From the EIS data (Table 8), we noted that the data of R_{ct} rise with rising the dose of the inhibitor and this lead to an rise in % IE. Data of capacitance double layer are also lower to the maximum inhibitor extent. The lower in CPE/C_{dl} data from a lower in local dielectric constant and/or an improve in the double layer thickness, given that HL protect the C38 steel from corrosion. The main advantages of EIS are to follow the corrosion behavior of the metal with constant time. The inhibition efficiency was calculated from the charge transfer resistance data from equation 15:[38]

$$\%IE_{EIS} = \left[1 - (R^\circ_{ct}/R_{ct})\right] \times 100 \qquad (15)$$

where R°_{ct} and R_{ct} are the charge-transfer resistance values without and with inhibitor, consecutively.

3.10.3 | EFM method

The advantages of EFM test give it an ideal for online monitoring of corrosion. The causality factors are higher strength data of the EFM which act as an internal check

TABLE 7 Concentrations parameters effect of HL for C38 steel in 2 M hydrochloric acid attendances and lack of unlike dose of inhibitor at 30 ± 1 °C

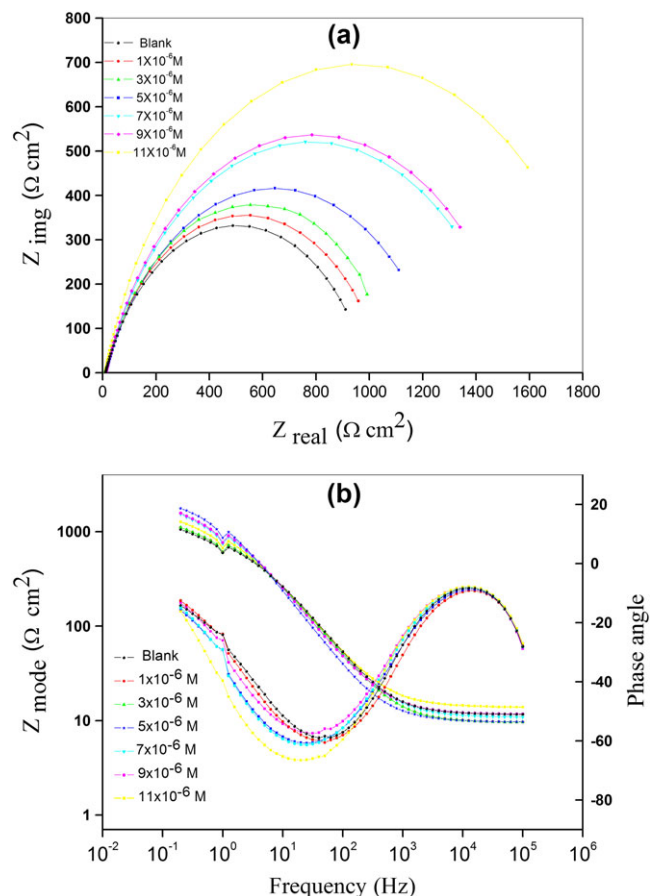| Conc., M.	-E_{corr} (mV vs. SCE)	$i_{corr} \times 10^{-5}$ (μA cm^{-2})	$\beta_a \times 10^{-3}$ (mV dec^{-1})	$\beta_c \times 10^{-3}$ (mV dec^{-1})	θ	% IE
Blank	455	2.56	82.6	202.5	-----	-----
1x10^{-6}	475	2.09	84.3	145.3	0.1835	18.35
3x10^{-6}	474	2.05	94.0	141.6	0.1992	19.92
5 x10^{-6}	448	2.01	71.2	197.2	0.2148	21.48
7x10^{-6}	434	1.84	42.5	107.2	0.2812	28.12
9x10^{-6}	474	1.83	83.5	127.1	0.2851	28.51
11x10^{-6}	494	1.06	112.7	151.4	0.5859	58.59

FIGURE 17 EIS Nyquist (a) and Bode diagrams (b) for the corrosion of C38 steel in 2 M hydrochloric acid attendance and lack of unlike dose of HL at 30 ± 1 °C

β_a). The EFM parameters were given in Table 9 show that, the appended of HL at a given dose to the acidic solution lower the current corrosion density, lead to these compounds protect the corrosion of alloy through adsorption. The best data of CF-2 and CF-3 in Table 9 are similar to their theoretical data of 2.0 and 3.0, respectively lead to the calculated value are quality good.

The % IE$_{EFM}$ improves by raising the inhibitor dose and was measured from equation 16:

$$\%IE_{EFM} = \left[1 - \left(i_{corr}/i^{o}_{corr}\right)\right] \times 100 \quad (16)$$

where i^{o}_{corr} and i_{corr} are current corrosion densities without and with inhibitor, consecutively.

3.10.4 | Mechanism of corrosion protection

From the electrochemical experiments the % IE relies on dose, metal nature, surface conditions and the type of inhibitor adsorption on C38 steel.

The results of corrosion value attendance of this inhibitor:

i. The lower of rate and current of corrosion with rise in dose of the inhibitor.
ii. The change in Tafel lines to maximum regions of potential.
iii. The lower in % IE corrosion with improve temperature lead to desorption of the adsorbed inhibitor molecules obtain.
iv. The %IE relies on charge density and their equipment of adsorption centers in the molecule.

It was observed that the type of adsorption relies on the affinity of the C38 steel towards the clouds of π-electron of the ring. Metals such as iron, which have a higher attract towards aromatic moieties, were obtain to adsorb benzene rings in orientation flat. HL exhibits excellent inhibition power due to its larger molecular size that may facilitate better surface coverage.

on verified data and of the EFM test. The CF-2 and CF-3 are record from the frequency spectrum of the responses current. The data of EFM in acidic solution with and without various doses of HL given in Figure 18. The two higher peaks, with amplitude of about 200 μA, are the given to the 40 and 100 mHz (2 and 5 Hz) excitation frequencies. The EFM experimental data were utilized two unlike models: diffusion complete control of the cathodic reaction and the 'activation' model. [48,49] The higher peaks were utilized to measure the (i_{corr}), (CF-2 and CF-3) and (β_c and

TABLE 8 Kinetic parameters given by EIS test for C38 steel in 2 M HCl attendance and lack of unlike dose of HL at 30 ± 1 °C

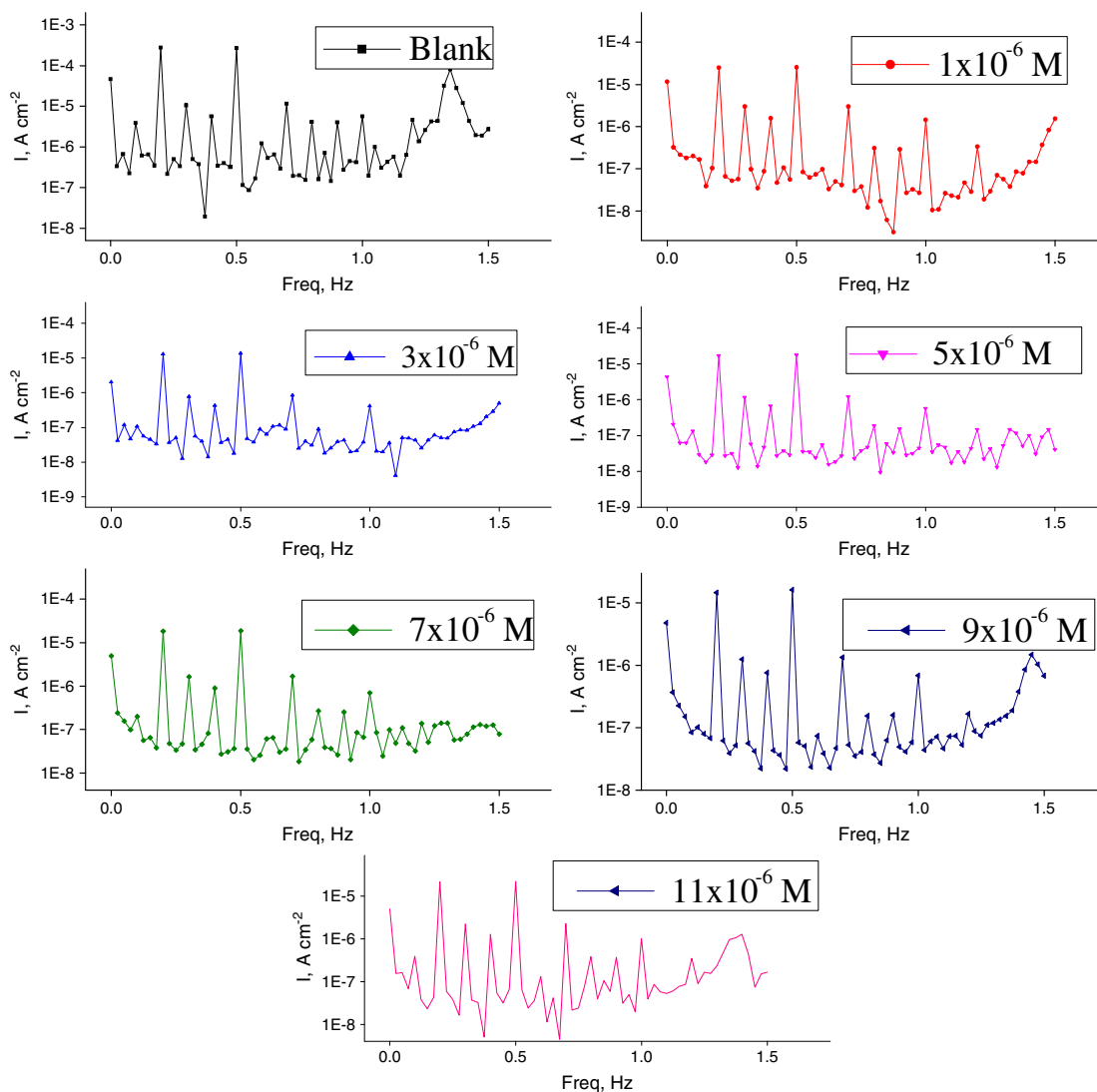| Conc., M.	$R_S \times 10^{-3}$ (Ω cm²)	$Y_o \times 10^{-6}$ (μΩ^{-1}s^n)	$n \times 10^{-3}$	R_{ct} (Ω cm²)	$C_{dl} \times 10^{-5}$ (μFcm^{-2})	θ	%IE
Blank	9.131	158.4	758.5	1.018	9.956	-----	------
1x10^{-6}	9.120	158.3	758.7	1.048	8.942	0.0286	2.86
3x10^{-6}	13.28	169.5	743.9	1.258	8.940	0.1907	19.07
5 x10^{-6}	10.51	167.0	758.1	1.538	8.570	0.3381	33.81
7x10^{-6}	11.35	157.7	769.4	1.557	1.099	0.3461	34.61
9x10^{-6}	9.49	148.8	807.5	1.892	1.082	0.4619	46.19
11x10^{-6}	11.00	156.8	755.6	1.985	1.035	0.4871	48.71

FIGURE 18 EFM spectra for the corrosion of C38 steel in 2 M hydrochloric acid attendance and lack of unlike dose of HL at 30 ± 1 °C

TABLE 9 Electrochemical kinetic parameters obtained by EFM technique for C38 steel in 2 M HCl without and with various concentrations of HL at 30 ± 1 °C

Conc., M.	i_{corr} (μA cm^{-2})	$\beta_{a \times 10^{-3}}$ (mV dec^{-1})	$\beta_{c \times 10^{-3}}$ (mV dec^{-1})	CF-2	CF-3	θ	%IE
Blank	101.20	107.9	85.4	1.93	3.12	-----	------
1×10^{-6}	57.24	327.3	96.5	1.98	3.45	0.4343	43.43
3×10^{-6}	38.77	297.5	140.9	1.89	3.23	0.6168	61.68
5×10^{-6}	36.68	190.0	105.6	1.93	3.27	0.6375	63.75
7×10^{-6}	35.36	188.8	92.6	2.07	3.06	0.6005	60.05
9×10^{-6}	33.62	225.7	104.4	1.78	3.04	0.6077	60.77
11×10^{-6}	32.86	147.2	75.6	1.95	3.14	0.6752	67.52

4 | CONCLUSIONS

The molecular structures, elemental analyses, IR spectra, spectral studies, molar conductance, magnetic measurements, mass spectra, X-ray diffraction analysis, thermal study and thermodynamics parameters of N-[4-(5-methyl-isoxazol-3-ylsulfamoyl)-phenyl]-acrylamide and its M(II) complexes. Monomer and its M(II) complexes are screened for their antimicrobial activity against bacteria and fungi species. It was found that Cd(II) complex

has more antibacterial activity than the penicillin against *Klebsiella pneumoniae*. From the values of the thermal activation energy for decomposition (E_a) of monomer and its polymer complexes, it was found that the E_a value for the complex (1) is higher compared to the other complexes. HL is good corrosion inhibitor for C38 steel in 2 M HCl solution. The effectiveness of this inhibitor depends on its structure. The variation in inhibitive efficiency depends on the type and the nature of the substituent present in the inhibitor molecule. Double layer capacitances decrease with respect to blank solution when the inhibitor added. This fact may explained by adsorption of the inhibitor molecule on the C38 steel surface. EFM can be utilized as a fast and nondestructive tests for calculation of corrosion without prior information of Tafel lines

ACKNOWLEDGEMENT

ORCID

A.Z. El-Sonbati http://orcid.org/0000-0001-7059-966X
M.A. Diab http://orcid.org/0000-0002-9042-1356
Sh.M. Morgan http://orcid.org/0000-0002-8921-4894

REFERENCES

[1] F. Al-Khodir, *Orient. J. Chem.* **2015**, *31*, 1277.

[2] M. G. Abd El-Wahed, S. M. El-Megharbel, M. Y. El-Sayed, Y. M. Zahran, M. S. Refat, *Bulg. Chem. Comm.* **2015**, *47*, 895.

[3] D. P. Patel, S. P. Prajapati, P. S. Patel, *RJPBCS 3* **2012**, 1.

[4] A. K. Stuck, M. G. Täuber, M. Schabel, T. Lehmann, H. Suter, K. Mühlemann, *Antimic. Agents Chemo.* **2012**, *56*, 1359.

[5] R. Singh, N. Gautam, A. Mishra, R. Gupta, *Ind. J Pharm.* **2011**, *43*, 246.

[6] S. P. V. Chamundeeswaria, E. J. J. Samuela, N. Sundaraganesanb, *Spectrochim. Acta A* **2014**, *118*, 1.

[7] A. Ashrafa, W. A. Siddiquia, J. Akbara, G. Mustafac, H. Krautscheidc, N. Ullahd, B. Mirzad, F. Shere, M. Hanifb, C. G. Hartingerb, *Inorg. Chimi. Acta* **2016**, *443*, 179.

[8] S. Medicia, M. Peanaa, V. M. Nurchib, J. I. Lachowiczb, G. Crisponib, M. A. Zoroddua, *Coord. Chem. Rev.* **2015**, *284*, 329.

[9] A. C. Tella, J. A. Obaleye, *Bull. Chem. Soc. Ethiop.* **2011**, *25*, 371.

[10] A. S. Abu-Khadra, R. S. Farag, A. Eldin, M. Abdel-Hady, *J. Appl. Chem.* (IOSR-JAC) **2015**, *8*, 67.

[11] M. A. Diab, A. Z. El-Sonbati, M. E. Attallah, *Coord. Chem.* **2012**, *65*, 539.

[12] M. A. Diab, A. Z. El-Sonbati, R. H. Mohamed, *Spectrochim. Acta A* **2010**, *77*, 795.

[13] A. Z. El-Sonbati, M. A. Diab, M. S. El-Shehawy, M. M. Makpel, *Spectrochim. Acta A* **2010**, *75*, 394.

[14] A. Z. El-Sonbati, A. A. Al-Sarawy, M. Moqbel, *Spectrochim. Acta A* **2009**, *74*, 463.

[15] A. Z. El-Sonbati, R. M. Issa, A. M. AbdEl-Gawad, *Spectrochim. Acta A* **2007**, *68*, 134.

[16] A. Z. El-Sonbati, A. A. M. Belal, M. A. Diab, R. H. Mohamed, *J. Mol. Struct.* **2011**, *990*, 26.

[17] A. Z. El-Sonbati, M. A. Diab, M. M. EL-Halawany, N. E. Salam, *Spectrochim. Acta A* **2010**, *77*, 755.

[18] A. Z. El-Sonbati, A. M. Belal, M. A. Diab, M. Z. Balboula, *Spectrochim. Acta A* **2011**, *78*, 1119.

[19] L. R. Kelland, *Eur. J. Cancer* **2005**, *41*, 971.

[20] R. S. Kumar, S. Arunachalam, V. S. Periasamy, C. P. Preethy, A. Riyasdeen, M. A. Akbarsha, *Europ. J. Med. Chem.* **2008**, *43*, 2082.

[21] M. M. El-Naggar, *Corro. Sci.* **2007**, *49*, 2226.

[22] G. Gece, *Corro. Sci.* **2011**, *53*, 3873.

[23] M. I. Abou-Dobara, A. Z. El-Sonbati, Sh. M. Morgan, *World J. Microbiol. Biotechnol.* **2013**, *29*, 119.

[24] A. Z. El-Sonbati, M. A. Diab, Sh. M. Morgan, *J. Mol. Liq.* **2017**, *225*, 195.

[25] P. W. Selwood, *Magnetic Chemistry*, Interscience Pub. Inc., New York **1956**.

[26] H. M. Refaat, H. A. El-Badway, Sh. M. Morgan, *J. Mol. Liq.* **2016**, *220*, 802.

[27] G. G. Mohamed, A. A. El-Sherif, M. A. Saad, S. E. A. El-Sawy, Sh. M. Morgan, *J. Mol. Liq.* **2016**, *223*, 1311.

[28] A. Z. El-Sonbati, M. A. Diab, Sh. M. Morgan, H. A. Seyam, *J. Mole. Struct.* **2018**, *1154*, 354.

[29] A. El-Dissouky, A. M. Hindawy, A. Abdel-Salam, *Inorg. Chim. Acta* **1986**, *117*, 109.

[30] A. S. Salameh, H. A. Tayim, *Polyhedron* **1983**, *2*, 829.

[31] K. Nakamoto, *Infrared and Raman Soectra of Inorganic and Coordination Compound*, Wiley, New York **1978**.

[32] M. Sebastian, V. Anm, P. P. Robinson, P. Leeju, G. Varsha, D. Varrghese, K. K. M. Yusuff, *Coord. Chem.* **2011**, *64*, 525.

[33] A. Z. El-Sonbati, A. A. M. Belal, M. S. El-Gharib, Sh. M. Morgan, *Spectrochim. Acta A* **2012**, *95*, 627.

[34] A. Z. El-Sonbati, M. A. Diab, A. A. M. Belal, Sh. M. Morgan, *Spectrochim. Acta A* **2012**, *99*, 353.

[35] Z. H. Chohan, H. A. Shad, F. H. Nasim, *Appl. Organometal. Chem.* **2009**, *23*, 319.

[36] F. A. Cotton, G. Wilkinson, *Advanced Inorganic Chemistry*, Vol. 869, Wiley Eastern, New Delhi **1972** 881.

[37] A. B. P. Lever, *Inorganic Electronic Spectroscopy*, Elsevier, Amsterdam **1968**.

[38] Sh. M. Morgan, A. Z. El-Sonbati, H. R. Eissa, *J. Mol. Liq.* **2017**, *240*, 752.

[39] E. Konig, *The Nephelaxetic Effect in Structure and Bonding*, Springer Verlag, Berlin, New York **1971**.

[40] R. K. Rao, P. S. Zacharias, *Polyhedron* **1977**, *16*, 1201.

[41] N. A. El-Ghamaz, A. Z. El-Sonbati, Sh. M. Morgan, *J. Mol. Struc.* **2012**, *1027*, 92.

[42] K. B. Gudasi, S. A. Patil, R. S. Vadavi, R. V. Shenoy, M. Nehaji, S. W. A. Biigh, *Inorg. Chim. Acta* **2006**, *359*, 3229.

[43] A. W. Coats, J. P. Redfern, *Nature* **1964**, *201*, 68.

[44] H. H. Horowitz, G. Metzger, *Anal. Chem.* **1963**, *35*, 1464.

[45] N. A. El-Ghamaz, M. A. Diab, A. Z. El-Sonbati, Sh. M. Morgan, O. L. Salem, *Chem. Pap.* **2017**, *71*, 2417.

[46] S. Thamizharasi, J. Vasantha, B. S. R. Reddy, *Eur. Polym. J.* **2002**, *38*, 551.

[47] A. S. Fouda, A. M. Eldesoky, A. Z. El-Sonbati, S. F. Salam, *Int. J. Electrochem., Sci.* **2014**, *9*, 1867.

[48] A. J. Trowsdate, B. Noble, S. J. Haris, I. S. R. Gibbins, G. E. Thomson, G. C. Wood, *Corros. Sci.* **1996**, *38*, 177.

[49] F. M. Reis, H. G. de Melo, I. Costa, *J. Electrochem. Acta* **2006**, *51*, 1780.